AFRL-AFOSR-VA-TR-2023

Superconducting Hybrid Plasmonics

Kieu, Khanh
UNIVERSITY OF ARIZONA
888 N EUCLID AVE RM 510
TUCSON, AZ, 85719
USA

02/22/2023
Final Technical Report

Air Force Research Laboratory
Air Force Office of Scientific Research
Arlington, Virginia 22203
Air Force Materiel Command

REPORT DOCUMENTATION PAGE

PLEASE DO NOT RETURN YOUR FORM TO THE ABOVE ORGANIZATION.

1. REPORT DATE	2. REPORT TYPE	3. DATES COVERED	
20230222	Final	START DATE 20150930	END DATE 20201231

4. TITLE AND SUBTITLE
Superconducting Hybrid Plasmonics

5a. CONTRACT NUMBER	5b. GRANT NUMBER	5c. PROGRAM ELEMENT NUMBER
	FA9550-15-1-0389	61102F
5d. PROJECT NUMBER	**5e. TASK NUMBER**	**5f. WORK UNIT NUMBER**

6. AUTHOR(S)
Khanh Kieu

7. PERFORMING ORGANIZATION NAME(S) AND ADDRESS(ES)
UNIVERSITY OF ARIZONA
888 N EUCLID AVE RM 510
TUCSON, AZ 85719
USA

8. PERFORMING ORGANIZATION REPORT NUMBER

9. SPONSORING/MONITORING AGENCY NAME(S) AND ADDRESS(ES)	10. SPONSOR/MONITOR'S ACRONYM(S)	11. SPONSOR/MONITOR'S REPORT NUMBER(S)
Air Force Office of Scientific Research 875 N. Randolph St. Room 3112 Arlington, VA 22203	AFRL/AFOSR RTB1	AFRL-AFOSR-VA-TR-2023-0280

12. DISTRIBUTION/AVAILABILITY STATEMENT
A Distribution Unlimited: PB Public Release

13. SUPPLEMENTARY NOTES

14. ABSTRACT
Program Objective: 1) To grow unique nanostructures on silicon substrates for different optoelectronics applications. 2) To study the mechanism of interaction of nanostructures with intense femtosecond laser pulses with emphasis on the time dynamics of nanostructure modification. Our Approaches: • Samples creation with Molecular Beam Epitaxy (MBE)
growth technique • Femtosecond laser focused onto nanostructures • Pump/probe technique is used to understand the time dynamics in fs time regime Benefits: • New laser-matter interaction physics • Creation of new materials under ultrafast laser interaction • Growth of new materials via in-situ femtosecond laser-assisted MBE growth • Ultrafast laser propulsion technology – achieving ultrafast acceleration and high speed in a very short time window • Education and training of graduate students Accomplishments: • We have done systematic study on the growth of indium nanostructures on silicon substrates and have achieved a very good understanding of their growth mechanism. We can now control the growth process to achieve targeted outcomes. We have also done growth on Si (111) substrate and saw new nanostructures that are formed following the orientation of the crystal axis of the substrate.
Detailed description of the growth process and results are discussed below. • We have published our initial results on the modification of Indium nanostructures or 'bubbles' with femtosecond laser pulses. The manuscript received very positive reviews and became the editor's pick for the journal's issue. ? The graduate student (Sander Zandbergen) involved in the research project has also defended his PhD thesis successfully over the summer and has just joined JPL in Pasadena as an Optical Engineer. ? We have also made significant progress in understanding the modification process of Indium islands under interaction with focused femtosecond laser pulses. These islands would not only elongate (with linear polarization) but also form multiple filaments depending on the energy of the femtosecond laser pulses. We also observed formation of multiple 'loops' of material when the islands are excited with circular polarization

15. SUBJECT TERMS

16. SECURITY CLASSIFICATION OF:			17. LIMITATION OF ABSTRACT	18. NUMBER OF PAGES
a. REPORT	b. ABSTRACT	c. THIS PAGE		
U	U	U	UU	43

19a. NAME OF RESPONSIBLE PERSON	19b. PHONE NUMBER *(Include area code)*
GERNOT POMRENKE	426-8426

Superconducting Hybrid Plasmonics

(Final Report of Modified Research Plan, grant FA9550-15-1-0389)

Khanh Kieu

College of Optical Sciences, University of Arizona

To: Dr. Gernot Pomrenke, Program Manager

Subject: Final Report

Contract/Grant #: FA9550-15-1-0389

Reporting Period: 9/30/2015 to 12/31/2019

Program Objective:

1) To grow unique nanostructures on silicon substrates for different opto-electronics applications. 2) To study the mechanism of interaction of nanostructures with intense femtosecond laser pulses with emphasis on the time dynamics of nanostructure modification.

Our Approaches:

- Samples creation with Molecular Beam Epitaxy (MBE) growth technique
- Femtosecond laser focused onto nanostructures
- Pump/probe technique is used to understand the time dynamics in fs time regime

Benefits:

- New laser-matter interaction physics
- Creation of new materials under ultrafast laser interaction
- Growth of new materials via in-situ femtosecond laser-assisted MBE growth
- Ultrafast laser propulsion technology – achieving ultrafast acceleration and high speed in a very short time window
- Education and training of graduate students

Accomplishments:

- We have done systematic study on the growth of indium nanostructures on silicon substrates and have achieved a very good understanding of their growth mechanism. We can now control the growth process to achieve targeted outcomes. We have also done growth on Si (111) substrate and saw new nanostructures that are formed following the orientation of the crystal axis of the substrate. Detailed description of the growth process and results are discussed below.

- We have published our initial results on the modification of Indium nanostructures or 'bubbles' with femtosecond laser pulses. The manuscript received very positive reviews and became the editor's pick for the journal's issue.
- The graduate student (Sander Zandbergen) involved in the research project has also defended his PhD thesis successfully over the summer and has just joined JPL in Pasadena as an Optical Engineer.
- We have also made significant progress in understanding the modification process of Indium islands under interaction with focused femtosecond laser pulses. These islands would not only elongate (with linear polarization) but also form multiple filaments depending on the energy of the femtosecond laser pulses. We also observed formation of multiple 'loops' of material when the islands are excited with circular polarization. We are very excited about these new results and are working on a new manuscript to report them (Please find more details in the progress report for 2017).
- We have studied the growth of indium nanostructures on silicon substrates (with both 100 and 111 orientation). We have observed that indium nanostructures are formed following the orientation of the crystal axis of the substrate. The growth process and control of nanostructure size and density are now well understood. Detailed description of the growth process and resulting nanostructures are discussed below.
- We have also investigated the morphology as well as composition of grown nanostructures using SEM, TEM and energy dispersive x-ray spectroscopy (EDX).
- We have also achieved significant progress in understanding the modification process of Indium islands under interaction with focused femtosecond laser pulses. These islands would not only elongate (with linear polarization) but also form multiple filaments depending on the energy of the femtosecond laser pulses. We also observed formation of multiple 'loops' of material when the islands are excited with circular polarization. We are have submitted a manuscript to Applied Physics Letters to report these new results.
- We have also performed experiment with 1030 nm femtosecond laser to study wavelength dependence effect. It turned out that similar elongation was also observed but the elongation length was much shorter compared to the case where a 1560 nm femtosecond laser was used.
- Significant effort has been devoted to understanding the underlying mechanism of the interaction between intense femtosecond pulses and the nanostructures. We have observed strong evidence that the effect may be closely related to the phenomenon of laser induced periodic surface structures that have been studied in the literature but its physical mechanism is still a topic for research.
- We have also started to investigate the possibility of using the modification process using femtosecond laser pulses to create useful devices such as nano-gratings and optical filter.
- We have built an ultrafast pump/probe laser system with dual wavelength output to study time dynamic of femtosecond laser nanostructure elongation process. This experimental setup is very challenging since it has single pulse measurement capability and diffraction limited resolution. Detailed description of the laser system will be discussed below since it has not been covered in previous annual reports.
- We have made significant improvement to our all-reflective microscope design to demonstrate their key advantages for dual-wavelength pump/probe spectroscopy/microscopy; namely, the removal of the effects of dispersion such as chromatic aberration and pulse spreading. The all-reflective architecture also easily supports wide range of laser wavelengths, enabling a compact and versatile new

instrument. Detailed description of the all-reflective microscope will be discussed below since it has not been covered in previous annual reports.

1. Dual wavelength fiber laser source

Our research group currently has multiple multi-photon microscopes that have been used to collect a significant amount of data from a variety of different samples. Such data has been useful for biological imaging, medical innovations and even insight into the structure of gemstones. Our lasers and microscope has also been used to study the mechanism of interaction of nanostructures with intense femtosecond laser pulses with emphasis on the time dynamics of nanostructure modification. While our current lasers enable such information to be attained with two and three photon non-linear processes, the subject of this work will be on the development of an additional laser source. This laser source's multiple wavelength output, broad tuning and all fiber format will lead to more versatility in our microscope setups and will allow us to do pump/probe spectroscopy with femtosecond time resolution with dual wavelengths.

While there are existing tunable ultrafast laser sources that can be used for pump/probe spectroscopy, they suffer from high complexity and cost, traditionally based on bulk Titanium-Sapphire (Ti:S) lasers. While these are robust and proven laser sources, there complexity to run and high cost has limited the ability of researchers to utilize this extremely desirable tool. A versatile, cost effective and simple laser source would open the doors for new applications, research and innovation. The goal of this work is to develop a cost-effective all-fiber laser source to provide researchers and scientists with an attainable instrument to fully take advantage of such an innovative spectroscopic/microscopic technique. We will show that an all fiber Ytterbium pumped OPO not only offers simplicity compared to that of Ti:S based systems but can provide greater tunability with comparable resolution. Additionally, we aim to demonstrate dual-wavelength pump/probe spectroscopy with high temporal resolution by this novel source.

The development of our all fiber laser system is a key element to enabling this simplified dual-wavelength pump/probe spectroscopy/microscopy device. The general concept of this laser is to generate two wavelengths from one single source which can then be combined for pump/ probe experiment. The work discussed below has built upon previous work done within our group. Multiple design considerations had to be considered to make this specific system well suited for this application. The laser system is divided up into four main parts: The mode-locked Ytterbium oscillator, a series of Ytterbium amplifiers, a secondary Ytterbium amplifier, and finally a Fiber Optical Parametric Oscillator (FOPO) for generation of the anti-stokes wavelength. Figure 1 shows

the schematic diagram of the full system, identifying the four segments that will be discussed in detail.

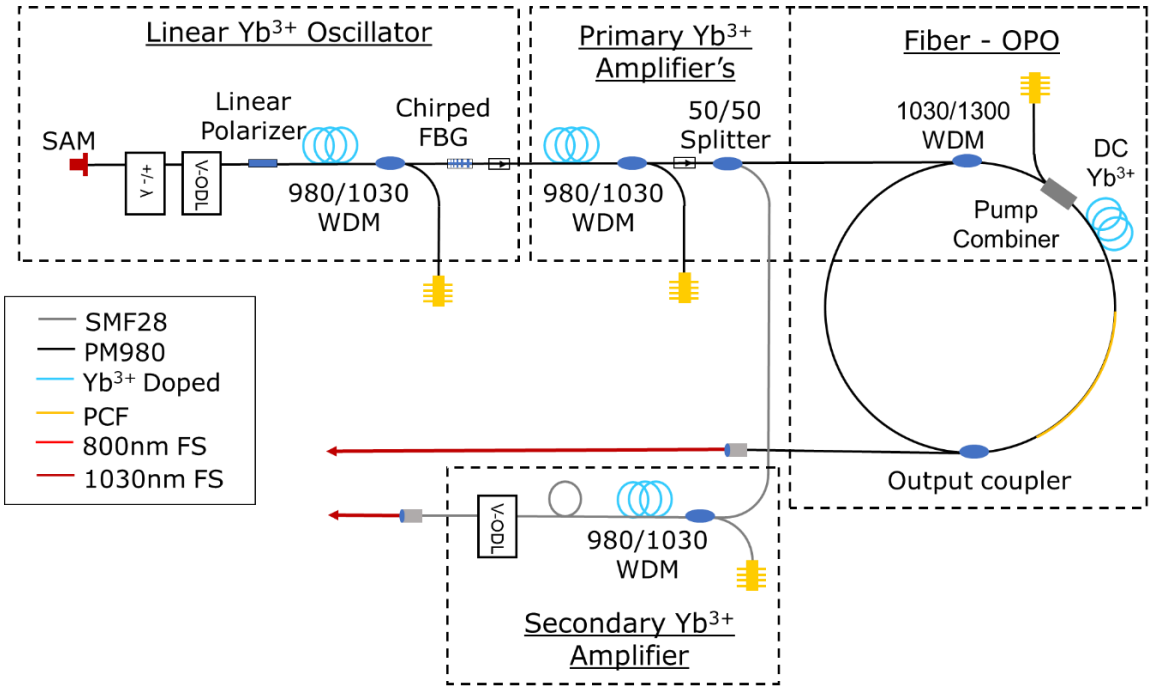

Figure 1: Full schematic of the two wavelengths pump/probe spectroscopy/microscopy laser constructed. The system is comprised of an Ytterbium oscillator, set of YDFA's and a FOPO.

Mode-Locked Ytterbium Fiber Oscillator

Description

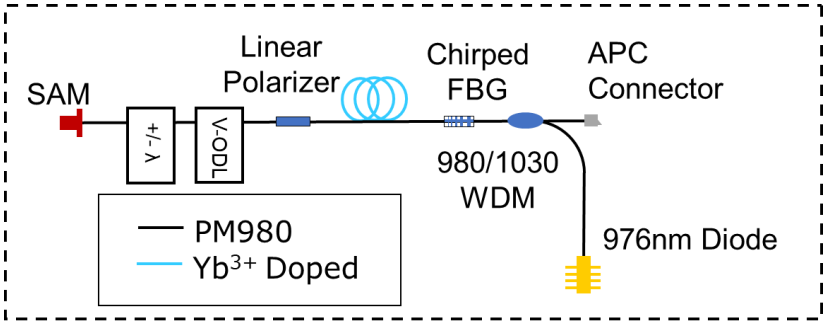

Figure 2: Schematic of the linear, mode-locked all PM Ytterbium fiber oscillator.

The front end of this entire laser system is that of the diode pumped linear mode-locked fiber oscillator. This oscillator provides the original low power 1µm seed which will be used throughout the rest of the system.

Figure 2 shows the schematic of the mode-locked Ytterbium oscillator producing the 1µm seed for this system. This is a low power oscillator which produces both temporally and spatially clean picosecond duration, megahertz repetition rate pulses.

A 976nm fiber coupled and wavelength stabilized laser diode controlled by a Wavelength Electronics LMD 1090 acts as the optical pump source for the oscillator. It is coupled into the cavity through a 980nm/1030nm wavelength division multiplexer (WDM) and a broadband 50% reflective Fiber Bragg Grating (FBG). The FBG acts as the output coupler for the cavity, while the WDM directs pump light into the cavity and the outcoupled light to the next stage of the system.

The laser oscillator is mode-locked by a Saturable Absorbing Mirror (SAM) from BATOP Optoelectronics. This device is comprised of a small semi-conductor grown atop of a mirror substrate. This is butt coupled to the end of a flat fiber connector with index matching gel, while a second flat fiber connector is used to apply pressure for good contact. Many different SAMs were tested in this system to find one working in the desired spectral tuning range and with the right response time.

The gain mechanism in this cavity is comprised of 60cm of Ytterbium doped gain fiber purchased from CoreActive. This fiber has a peak absorption around 976nm and emission between 1020nm – 1055nm. Because the emitted 1μm light is not polarized while the rest of the cavity is Polarization Maintaining (PM), a fiber coupled linear polarizer is inserted into the cavity after the gain fiber. This Ytterbium fiber has very high gain, so long segments of gain fiber are not necessary.

There are two other important components in this cavity. First, the wavelength tuner is a fiber coupled tunable grating purchased from Agiltron Inc. which allows central wavelength tunability of the oscillator. This is the main response tuning mechanism for the entire system. The second component is the delay line. The delay line allows cavity length tunability (thereby its repetition rate tunability) which helps in synchronously pumping the FOPO.

Characterization

The pump diode, purchased from 3S photonics, was characterized to confirm manufacturer specified performance before integration into the oscillator. The Light/Current (LI) curve can be seen in Figure . The shape is linear, as expected, and an output of 589.5mW can be attained with 912.5mA of current. The slope efficiency of this diode is 70.2% which corresponds to the manufacturer's specifications. This output power is more than enough to pump the oscillator and the first primary amplifier stage. The spectrum can be seen in Figure 3. It is centered at 975.6nm and has a linewidth of 0.4nm at -3dB.

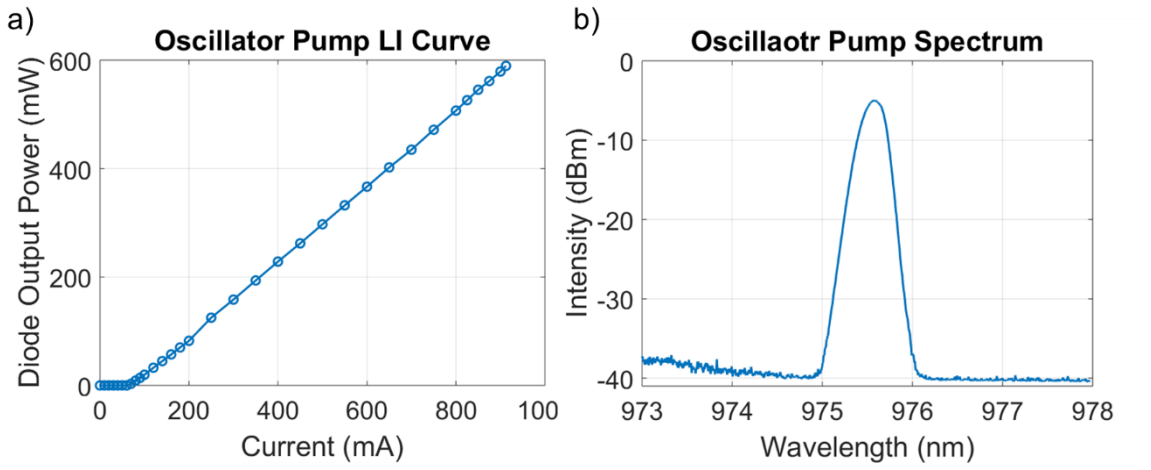

Figure 3: a) The Light/Current curve of the pump diode. b) The pump diode emission spectrum.

The mode-locked oscillator spectrum can be seen in Figure 4. This data was gathered from an Anritsu OSA. Figure a shows a zoomed in spectrum centered at 1039nm. The mode-locked laser spectrum has a -3dB linewidth of .3nm - .4nm. Figure b also shows the tuned mode-locked laser spectrum. Tunability was achieved from 1026nm to 1052nm while still maintaining stable mode-locking.

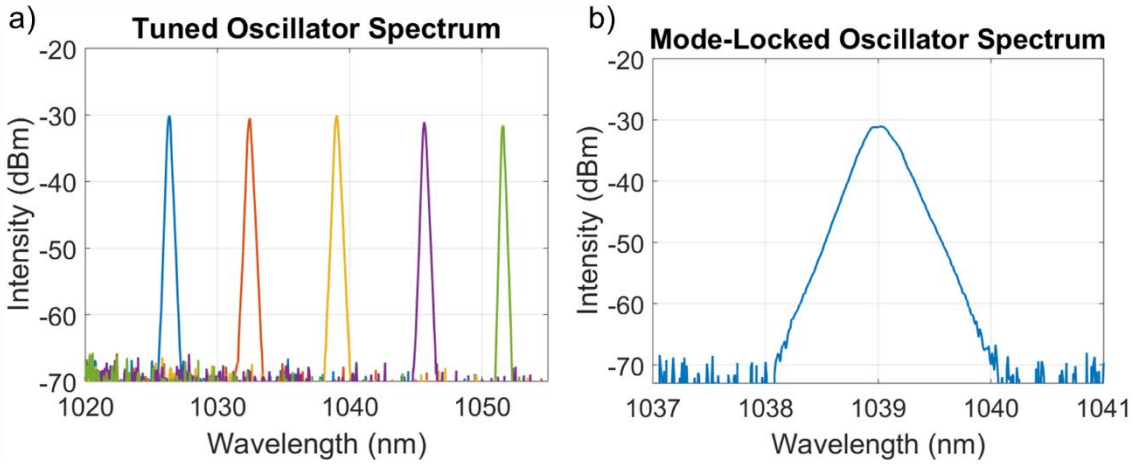

Figure 4: a) Zoomed in spectrum of the laser after mode-locking at 1043nm displaying the expected triangular shape. b) Multiple mode-locked spectral peaks tuned from 1026nm to 1052nm.

In order to characterize the pulse dynamics, a 100MHz fast photo-diode, 500MHz oscilloscope, and GHz frequency spectrum analyzer were utilized. Figure a shows the pulse train from the oscillator while Figure b shows a single peak at the repetition rate of the laser. The repetition rate, measured in both the time and frequency domain, was found to be 21.67MHz, corresponding to a cavity length of ~9.48m (assuming a constant n=1.46 refractive index throughout the fiber cavity).

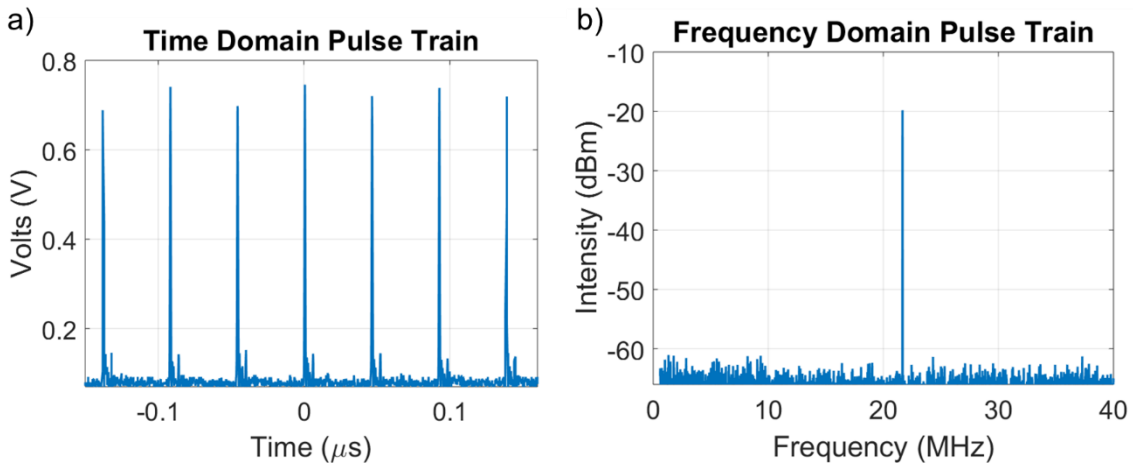

Figure 5: a) Oscilloscope trace of the oscillator pulse train. b) Frequency spectrum analyzer of the pulse train showing a rep-rate of 21.67MHz.

The current oscillator is only self-starting in the double pulsing regime. For this reason, starting the oscillator is achieved by increasing the pump diode current until double pulsing occurs, then lowering the current until the single pulsing regime. From this regime, the following data in Table 1 was collected. Continuous wave (CW) operation was achieved at 42.5mW input power. The upper pump threshold was found to be ~72.0mW and the oscillator would stay mode-locked after lowering the power down to ~54.0mW due to hysteresis. After much experimenting, it was determined that the oscillator ran most stable with at a pump power of ~62.2mW. The oscillator would stay stably mode-locked for >10 hours at this running point.

	CW	**Lower ML**	**Upper ML**	**Run Point**
Controller Volts (V)	.273	.310	.375	.342
Input Power (mW)	42.5	54.0	72.0	62.2
Output Power (mW)	.04	.9	1.3	1.2

Table 1: Characterization of the pump diode voltages, power and oscillator power for various oscillator running regimes.

Primary Ytterbium Fiber Amplifiers

Description

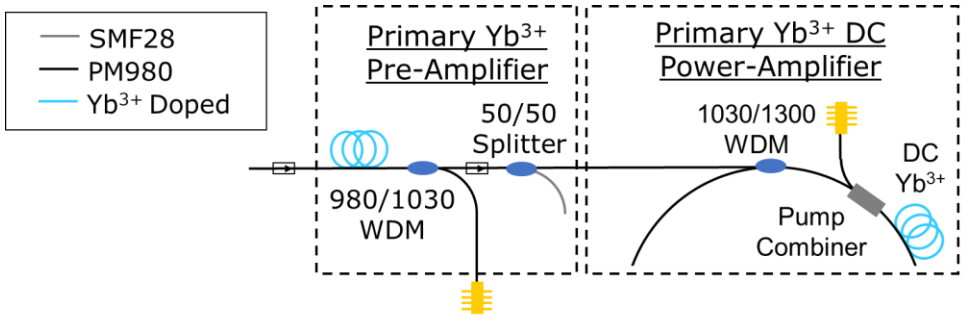

Figure 6: Schematic of the primary Ytterbium fiber amplifiers chain including the splitting of the signal for the secondary Ytterbium amplifier.

In order to properly seed the FOPO, the low power 1µm oscillator signal must be amplified. Not only is there a threshold to the parametric gain, but a certain amount of stokes light must be generated to excite the Raman response of our sample. Two stages of Ytterbium fiber amplifiers (YDFA) are implemented to accomplish this. The first stage is a counter pumped pre-amplifier and the second stage is a co-pumped high-power double-clad amplifier. Figure 6 shows the schematic of the amplifiers.

The first stage pre-amplifier is pumped by a second 976nm fiber coupled and wavelength stabilized diode. This diode is wired to a Newport 8000 Diode controller to run the drive current and Thermo Electric Cooler (TEC). In the final packaged system, this diode will not be needed, as a portion of the power from the oscillator pump will be split off to pump this pre-amplifier. The current pump was characterized up to 400mA of drive current, corresponding to 208mW of pump power. The rest of the amplifier is comprised of Ytterbium gain fiber and a 1064nm isolator to prevent any reverse propagating signals from disturbing the oscillator.

50% of the signal from the pre-amplifier is split off and sent to the secondary Ytterbium amplifier, the reason for this will be explained further in the corresponding section. The remaining 50% was sent to the power amplifier. This seed travels through a 1030nm/1300nm WDM which is part of the FOPO ring cavity, then a high-power pump combiner is used to combine the pre-amplifier seed and the high-power, multi-mode fiber coupled pump diode. This pump diode is wired to the second channel of the Newport 8000 Diode controller. This diode can provide up to 9W of output power. For the purposes of this system, it was characterized up to a 4.8A drive current with a corresponding output power of 2.76W, more than enough to amplify our seed for the FOPO.

The resulting power and spectral broadening are the two key factors that must be considered while constructing these amplifiers in order to have an efficient and powerful enough FOPO. Custom made high-efficiency large mode area double clad Ytterbium gain fiber was used as the gain medium for high-power amplification with these factors in mind. Double-clad (DC) gain fiber allows for high power pump light to be coupled into the core and first cladding. The seed propagates in the core but sees gain from all the excited ions in the core and first cladding. Originally, 1.1m of this gain fiber was used. This led to an efficiently working amplifier, but, unfortunately, the large length of gain fiber led to significant Self Phase Modulation (SPM) and therefore significant spectral broadening. Because we wish to run this FOPO narrow-band, this broadened seed causes problems with both the resulting bandwidth of the idler and the efficiency of parametric conversion. In order to reduce the SPM, the length of the DC gain fiber was reduced. While this decreased the efficiency of the amplifier, it reduced the SPM by nearly half. Because this is a low power FOPO system, we are willing to sacrifice the amplifiers efficiency for a less broadened spectrum. The original amplifier was constructed outside the FOPO cavity, but after realization that any length of fiber the amplified seed traveled through would add to the accumulated SPM, the high-power amplifier was moved into the FOPO cavity so that the narrowest possible amplified signal would see the parametric gain fiber. It should also be noted that because the core of the gain fiber is 10μm in diameter and that of the rest of the fiber in the cavity is 6μm, a fiber bridge must be constructed to get efficient power throughput to the PCF. This particular bridge was constructed by splicing a 1cm length 8.5 μm in-between the gain fiber and the next piece of PM980.

Characterization

The power and spectral characterization of the pre-amplifier can be seen in Figure . Nearly 40mW of output power from 200mW of input power could be achieved. The slope efficiency of this amplifier was found to be only 24%. This low efficiency is suspected to be because the seed from the oscillator passes through a 1064nm isolator. The specifications for this isolator show it has high loss outside 1059nm – 1069nm. Due to this, it is believed that the pre-amplifier is not fully saturated and that the replacement of this component with a broadband isolator would fix this problem. In addition to the amplifier's inefficiency, it should also be noted that the amplified signal passes through a second 1064nm isolator after the amplifier where an additional 40% loss occurs.

Along with the power, the spectral characteristics of the pre-amplifier were also evaluated. It can be seen in Figure b that very little spectral broadening was observed after amplification. Even at the greatest pumping power the spectrum expanded only to 0.62nm at -3dB.

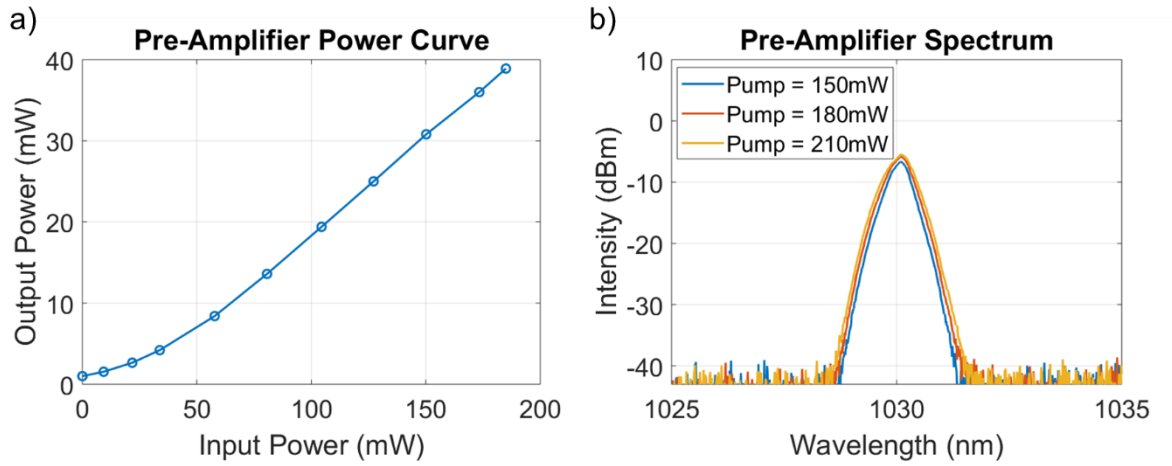

Figure 7: a) Input-Output characterization of the primary pre-amplifier. b) Spectral characterization of the primary pre-amplifier for varying pump powers.

After passing through the isolator, the pre-amplifier output is sent through a 50/50 coupler where ~10mW is output from each arm. One arm is passed through the FOPO WDM and pump combiner where ~9mW of signal remains to and is seeded into the power-amplifier. This is enough to saturate the DC-YDFA.

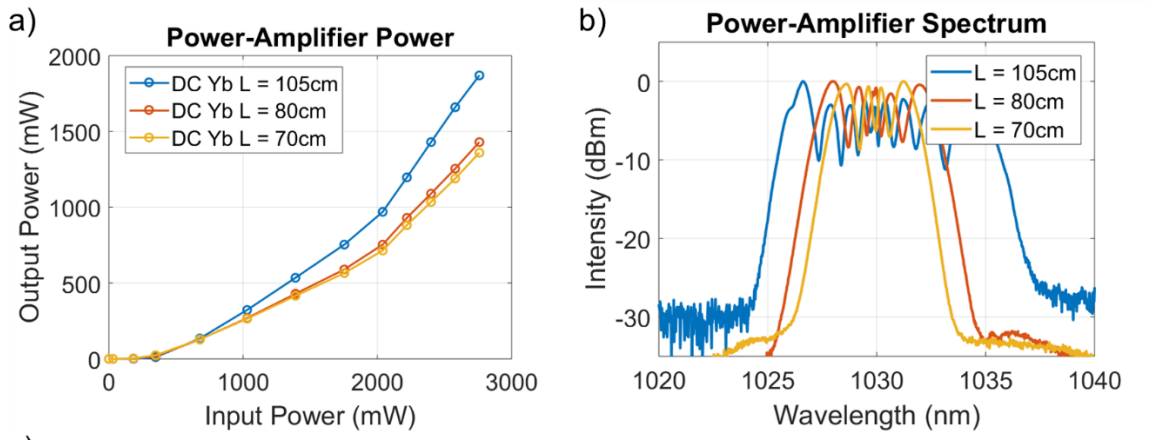

c)

DC Yb Length (cm)	Slope Efficiency (%)	Overall Efficiency (%)	Linewidth (nm)
105	82.6	67.8	8.5
80	61.6	51.8	6.2
70	58	49.3	4.15

Figure 8: Characteristics of the power amplifier at varying gain fiber lengths a) Input-Output curves. b) Spectra. c) Table summarizing efficiencies and linewidths.

As mentioned in the prior section, the power-amplifier was originally constructed with 1.1m of DC Ytterbium gain fiber. While this resulted in a very respectable slope efficiency of 82.6%, SPM in this length of fiber resulted in a linewidth of 8.5nm. In order to reduce the linewidth, the amplifier gain fiber length was cut back from 105cm to 80cm and finally to 70cm. The resulting power curves and spectra are shown in Figure . While reducing the gain fiber length reduced the slope efficiency from 82.6% to 58%, it also reduced the linewidth from 8.5nm to 4.15nm. Because the goal of this FOPO is not a high-power output, we are willing to sacrifice some efficiency for a narrower spectrum. There is of course a limit set by the parametric gain threshold and the desired output power in the idler. By reducing the gain fiber length to 70cm, the spectral linewidth is reduced by nearly half it was at 105cm, while still providing more than 1W of output power, which should still be enough.

Secondary Ytterbium Fiber Amplifier:

Description

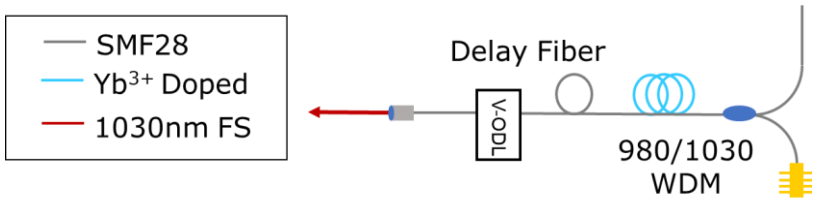

Figure 9: Schematic of the secondary Ytterbium fiber amplifier.

The first of two wavelengths produced from this laser source to induce Raman excitation in the microscope samples is that of the 1µm seed. While the resulting FOPO will output residual 1µm pump light, this signal is broader than desired and may drift off, in time, from the 1.3µm stokes signal. For both reasons, a portion of the 1µm seed is split off before the FOPO cavity and re-amplified in a secondary YDFA. This signal is then precisely delayed to over-lap in time with the generated 1.3µm stokes signal.

The secondary pre-amplifier is non-PM, comprised of Lucent-980 fiber and CoreActive Yb-402 gain fiber. It is co-pumped by a 976nm diode. After amplification, the amplified signal is delayed, in order to overlap with the FOPO generated stokes signal.

Characterization

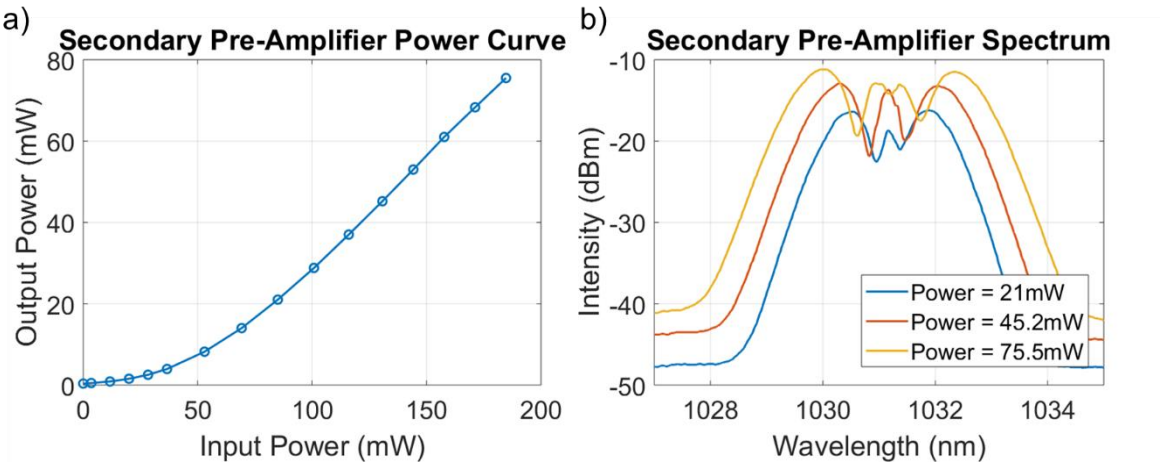

Figure 10: Input-Output characterization of the secondary pre-amplifier. b) Spectral characterization of the secondary pre-amplifier for varying pump powers.

The secondary pre-amplifier power and spectral characteristics are displayed in Figure . 75mW of 1µm signal was generated from 185mW of pump power, corresponding to a slope efficiency of 54.2%. The 75mW signal has a linewidth of 3.3nm. This linewidth will work well for high resolution of the induced Raman response.

All Fiber Optical Parametric Oscillator

Description

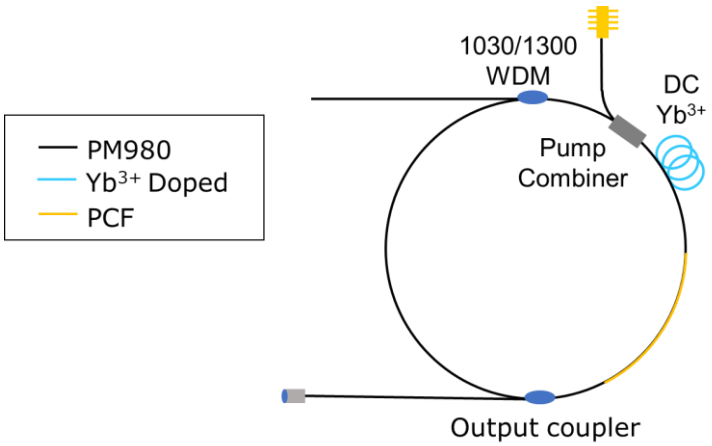

Figure 11: Schematic of FOPO including the high-power YDFA incorporated within the cavity.

The all fiber Optical Parametric Oscillator is the wavelength conversion mechanism of this laser system which is used to generate the second signal for use as the probe in our pump/probe experiment. This oscillator will generate a blue shifted signal and a red shifted idler. For this project, we take advantage of the idler which will be re-combined with the secondary amplified

1µm pump. The 1µm secondary pump and the 0.8µm signal can also be used for Raman or other multi-photon applications.

This OPO takes advantage of the χ^3 nonlinearity of fiber. In order to generate a good FOPO, a fiber with zero dispersion near the pump must be used. No standard fibers exist which have this property, so dispersion engineered, Photonic Crystal Fiber (PCF) is used as a phase matching mechanism. The oscillator itself is an all fiber ring cavity made from the power amplifier, PCF, outcoupler, WDM and meters of PM980. The schematic of this oscillator can be seen in Figure 11.

Simulation

The LMA5-PM PCF is well characterized in has been reported by us and other research groups. A MATLAB program, which was written by our group, based on this paper was utilized to determine the phase matching conditions and gain curves of this system. The relevant equations, which describe this, are as follows:

$$2)\ \Omega(\omega_p) = \left(\frac{-P(\omega_p)}{2} + \sqrt{\left(\frac{-P(\omega_p)}{2}\right)^2 - \frac{-24\gamma P_p}{\beta_4}}\right)^{1/2}$$

$$3)\ P(\omega_p) = 12\,\frac{\beta_3}{\beta_4}\,(\omega_p - \omega_0) + 6\,(\omega_p - \omega_0)^2$$

Where Ω is the parametric frequency shift, P_p is the pump power, β_3 and β_4 are the 3rd and 4th order dispersion, ω_p the pump frequency and ω_0 is the zero-dispersion frequency of the parametric gain fiber.

It can be seen from these equations that the gain is affected primarily by the pump power, pump wavelength and 3rd/4th order dispersion. The wavelength and power are used to tune that output, as the dispersion of the PCF is set. The phase matching and gain curves can be seen in Figure 1.

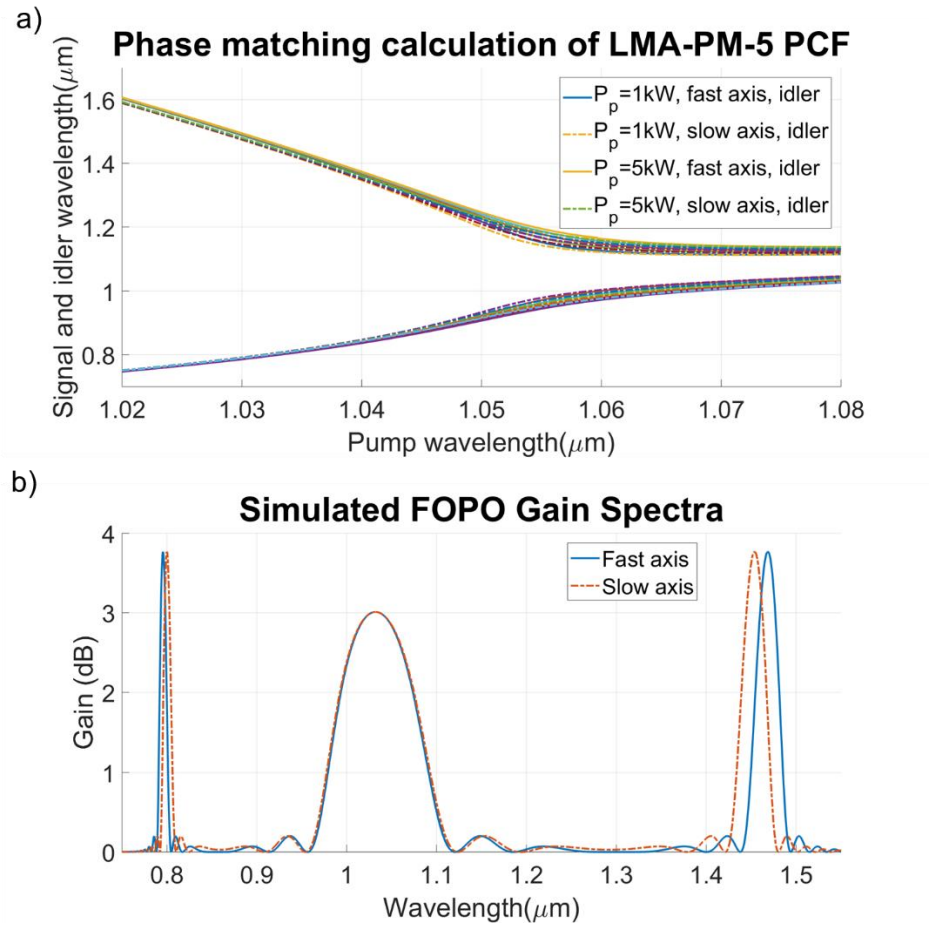

Figure 12: a) Phase matching curves for LMA5-PM PCF for varying pump wavelength and power. b) The simulate gain curves for the signal and idler with a 1032nm pump.

Figure 1 a) shows the phase matching curves for LMA5-PM PCF with a 1032nm pump. The desired idler wavelengths we are looking for in this system, 1.3µm -1.5µm, are mainly affected by pump wavelength as opposed to the pump power. Therefore, pump wavelength is the primary tuning mechanism. The gain curves shown in Figure 1 b) confirm that there will be significant gain for our desired wavelengths.

Construction

For this FOPO, LMA-PM5 PCF, from NKT photonics, was the specific PCF used. The rest of the cavity is comprised primarily of PM980 and some PM1550. The overall dispersion of this cavity is normal.

Both signal and idler resonant OPO configurations were constructed, by changing the WDM from a 1030nm/800nm to 1030nm/1300nm. It was shown that idler resonate FOPO's generated a narrower band signal and idler. This is commensurate with the results of previous work in our group. It should also be noted that the primary power amplifier was located inside the FOPO cavity.

This configuration was chosen for two reasons. First, little attenuation occurred between the amplifier and the phase matching medium. Second, this limits SPM that is added to the amplified 1μm pump, thereby reducing spectral broadening, before the phase matching medium. The pumps narrow spectral width is important to the efficiency and narrow linewidth of the generated signal and idler.

Multiple out-couplers were also tested. The FOPO is a relatively high gain system and it was determined that larger out-coupling, low feedback was best. A custom out-coupler designed to have an out-coupling ratio of 90/10 at 1300nm was finally used.

The length of this cavity is very important and extremely sensitive. The round-trip time of the resonating pulse in the OPO must be the same as that of the oscillator. By doing this only one pulse is in the cavity at a time and the resonating pulse perfectly overlaps with the next input pulse. This scheme is referred to as synchronous pumping and is a key requirement for parametric gain. The repetition rate of the oscillator was previously shown to be ~21.67MHz, this corresponds to 9.48m assuming a constant refractive index of 1.46. The delay line in the oscillator is capable of adjusting the cavity length by ± 5cm. This is not a significant amount of freedom with 9.48m of fiber. In order to accurately match the cavity lengths, the following electrical/time domain observation approach was taken.

1) The filter based micro-optics WDM in the FOPO was replaced with any fused based fiber component (Couplers works well). This was done to allow the 1μm pump signal to propagate.
2) The output of the FOPO was coupled to a highly-sensitive photo-diode connected to 1 port of a fast oscilloscope.
3) A tap from the oscillator was sent to a second photo-diode which is connected to the trigger port of a fast oscilloscope.
4) The FOPO cavity length was set to a few meters less than the expected length. By doing this one can observe the oscillator pulse and the FOPO resonant pulse separated on the oscilloscope.
5) From here small amounts of fiber were spliced into the cavity and the change in pulse separation was noted each time to build up confidence in the electrical observation corresponding to the actual added fiber.
6) Once the difference between the oscillator and FOPO resonate pulse were less than 1m in fiber length, the fused based fiber component was removed, and the filter-based WDM was re-inserted with fiber lengths equal to that of the removed fused component

plus the last difference in fiber length measured on the oscilloscope. Special accommodation should also be taken for the loss in fiber that will come from the cleaves made to splice this component into the cavity.

The synchronously pumped scheme described previously is a specific case referred to by the ratio 1:1, where only one pulse resonates in the cavity at a time. Other multiplicative lengths of the FOPO will also meet the condition of parametric gain. This is accomplished by increasing the FOPO length to any multiple of the oscillator. Such cases are referred to as 1:# of resonant pulses in the FOPO such as; 1:2, 1:10 or 1:100. The reason this can be useful in a fiber based OPO is that this increase in length changes the cavities overall dispersion. The dispersion is a key factor that changes the chirp of the resonant pulse as it propagates, and this plays a large role in the generated spectra and efficiency. While the current configuration is 1:1, a larger ratio synchronous pumping scheme may be investigated in the future to generate narrower linewidth idler spectra for greater resolution spectroscopy/microscopy.

Two different length of PCF were also tested, 20cm and 50cm. A few observations were determined from these two different cases. As expected, longer PCF decreased the OPO threshold. What was interesting though is that it did not necessarily increase the conversion efficiency. The major problem found with longer PCF is that, due to the extremely high non-linearity of this fiber, after certain pump powers were reached the spectra became very broad from the signal to the idler. This broadband effect is not desired but higher power is, so the longer PCF became a limiting factor in the desired performance of this system. It is possible that with the desired narrower band pump, this may be less of a problem.

Characterization

The full generated spectra from the FOPO described above can be seen in Figure 2 a). The spectra correspond to the simulated gain spectra found in the simulations. This confirms OPO operation. The central wavelength of the generated signal and idler was adjusted primarily by tuning the pump wavelength. Some further tunability is accomplished by adjusting the oscillator cavity length (adjusting the specific pump wavelengths synchronously pumped) but this was found to be most useful in fine tuning the shape of the spectra due to the modulation atop of the relatively broad pump. Figure 2 b) & c) show the zoomed-in spectra of the signal and idler respectively. It can be seen from the legend that the linewidth of the signal ranges from 2.5nm – 7.2nm and that of the idler from 4nm – 6.4nm. With the linewidth of the pump from the secondary amplifier being 2.4nm, the Raman response resolution corresponds to xxx for the signal and xxx for the idler. This is on par with current literature but, as mentioned previously, further narrowing of spectral

linewidth may be achieved. A very impressive characteristic of this system is its wide tunability. The signal was tuned from 779.2nm to 888nm and the idler from 1269.6 to 1507.3nm while still maintaining the desired linewidth.

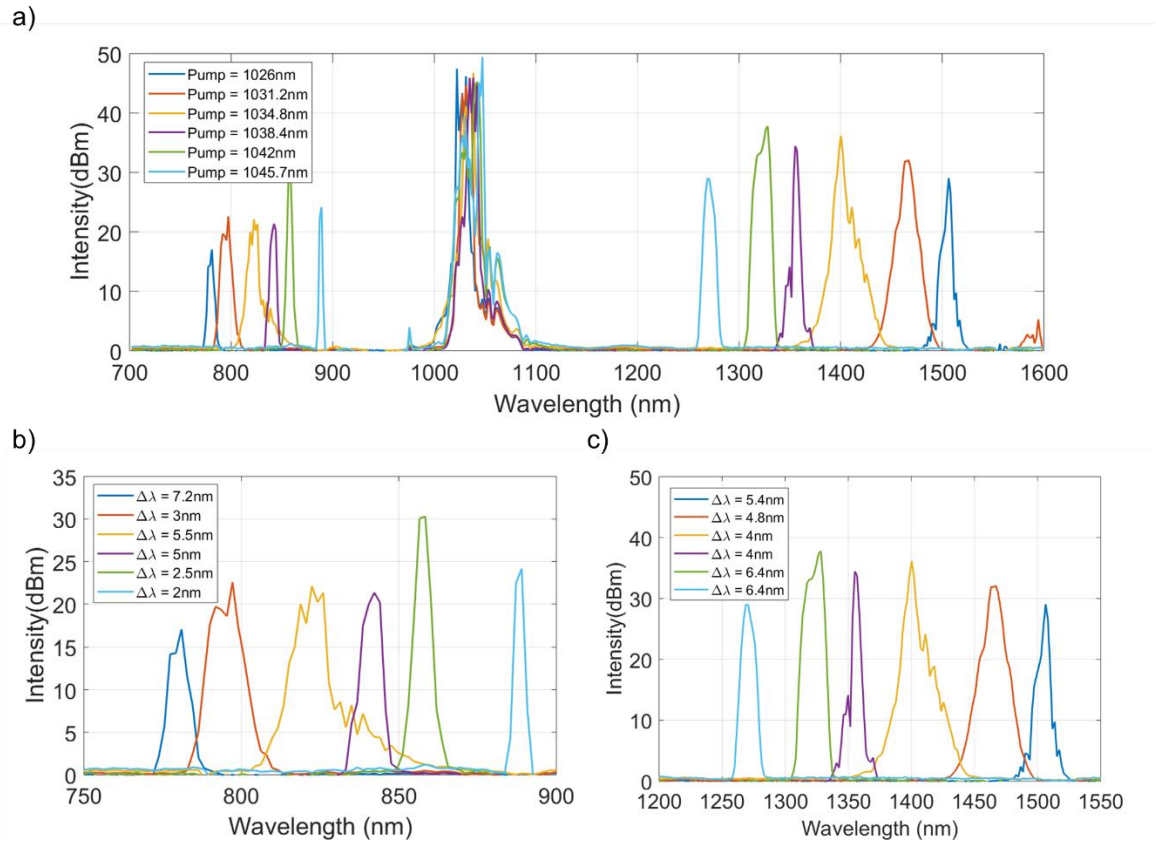

Figure 23: a) Full spectra of the pump, signal and idler generated by tuning the pump wavelength. b) Zoomed in spectra of the generated signal as the pump wavelength was tuned. c) Zoomed in spectra of the generated idler as the pump wavelength was tuned.

The power characteristics of the idler, which will be used in Raman microscopy, is summarized in Figure . The output power varies at different idler wavelengths and can be attributed to the phase matching. In general, the output power of the idler is lower than desired for Raman microscopy, less than 20mW even at 1W of pump power. This translates to ~1% conversion efficiency to the idler. It is believed this low conversion efficiency is due to the large spectral linewidth of the pump. Because the power of the pump is distributed over a large linewidth, and the chirp of this system is designed for narrow linewidth, only a portion of the 1W of pump gain is phase matched and converted to the signal and idler.

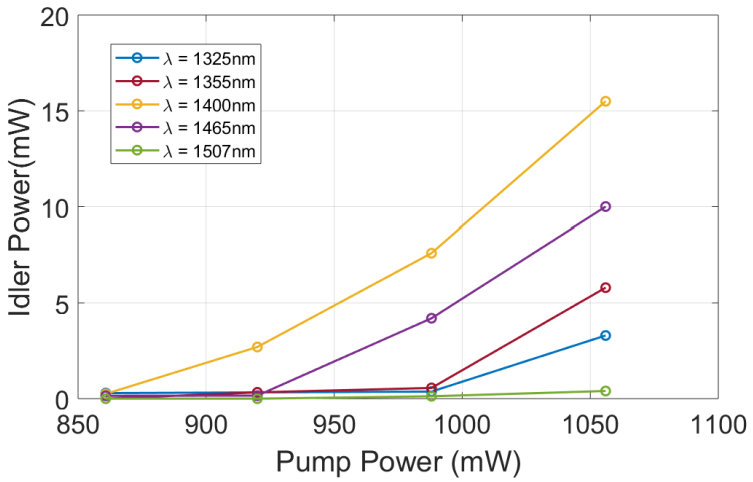

Figure 14: Power curves of Idler at various wavelengths from 1μm pump.

Laser Development Summary

The preceding sections show a successful construction of an all fiber OPO with multiple, relatively narrow band, output wavelengths. The system was constructed in four distinct parts specifically for the purpose of dual-wavelength pump/probe spectroscopy/microscopy. However, it was pointed out that improvements should be made to improve the linewidth and output power. While measures were taken to reduce SPM (reduction of gain fiber and placement of the amplifier just before the PCF) it is still too large for efficient conversion. The SPM effect is proportional to the intensity of light in the core of the fiber. In order to mitigate this problem, a larger core gain fiber, 20μm will be implemented. We expect this will increase the area by a factor of 4, also reducing the intensity by 4. We expect this will significantly decrease the SPM and increase the parametric conversion efficiency, while simultaneously decreasing the idler linewidth.

2. Improved all-reflective microscope

The design of a new mirror-based multi-modal microscope is presented in this chapter, dubbed the many mirrored multi-modal multiphoton microscope, or M6 for short. Our previous work has motivated the need and advantages of this type of multi-modal all reflective system well, so this part will focus entirely on the design and characterization of this system.

Design Requirements

The primary design requirements that guided this microscope are listed below.

(1) The system shall expand the input laser beam to fill the back aperture of the largest

microscope objectives in the lab, or 16 mm.

(2) The system shall support a $\pm 5^{\circ}$ FFOV.

(3) The system shall be able to utilize brightfield, multiphoton, and pump/probe spectroscopy/microscopy.

(4) The system shall automatically capture images and switch between modalities.

(5) The system shall be easy to align.

(6) The system shall be easy to assemble.

(7) The system should support a $\pm 10^{\circ}$ FFOV.

(8) The system should automatically change filters to adjust the laser beam power or wavelength with user input.

Several of these requirements are motivated by past designs. The previous all-reflective microscope was difficult to align and assemble, motivating the desire for a system that is simpler. The functional requirement on the beam expansion required that the microscope system expand the laser beam by a factor of 4 if the existing reflective collimators were used, as they presented a 2 mm beam.

OpticStudio Analysis

Initial designs similar to the previous all-reflective system were pursued, including the tri-Schiefsplieger telescope. To further simplify the system, two-mirror designs were pursued as well. A two-mirror system was created that met the requirements, but with performance worse than 2x the diffraction limit (Fig. 15). In addition, this system faced the same possible concerns as the previous ARMPM with the beam clipping on the mechanics of the galvometric mirrors as the light was focused past the mirror housing after reflecting off of the first mirror.

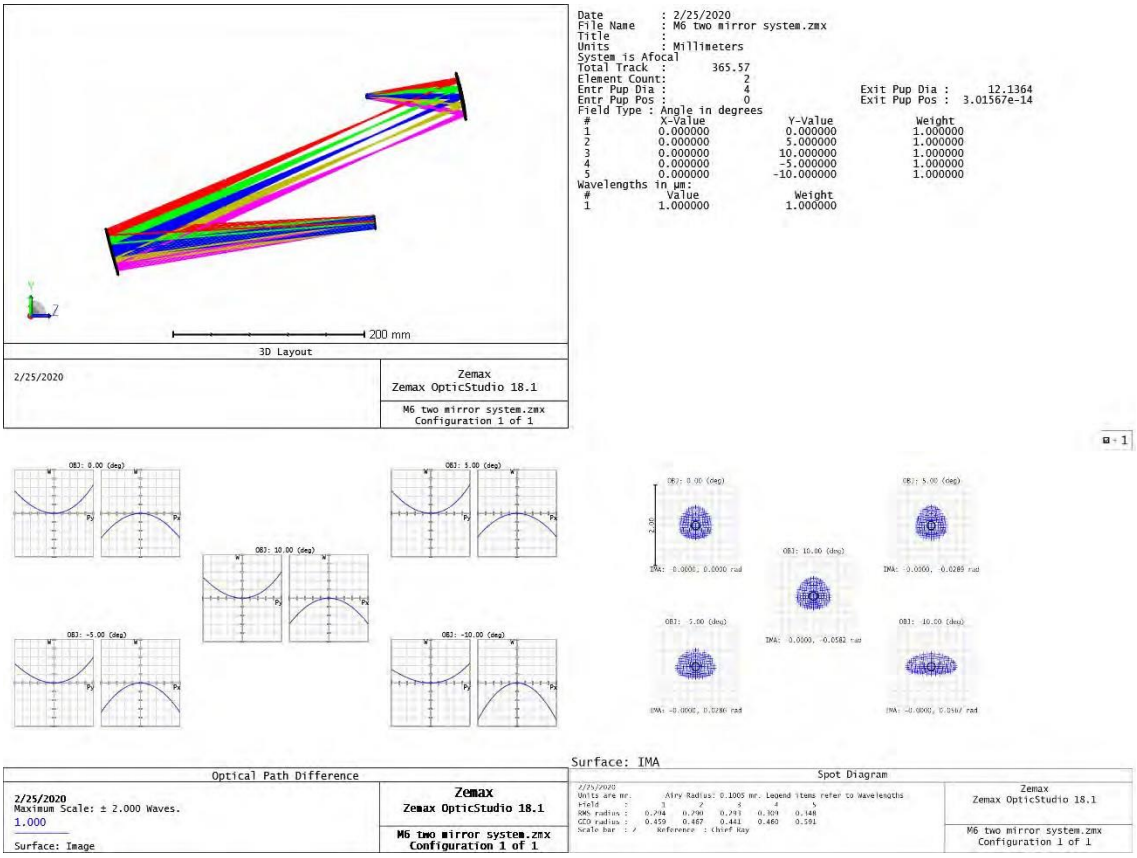

Figure 15: A summary graphic with the two-mirror design. This did not satisfy the performance metrics, as seen from the spot diagrams and OPD curves.

To keep this form factor, but improve performance, off-the-shelf off-axis parabolic (OAP) mirrors were chosen from the Thorlabs catalog and used in the system. A 2” focal length and 8” focal length parabola together met the beam expansion re- quirements. A Zemax OpticStudio diagram of the design is shown below in Fig. 16.

This system is diffraction limited up to a 10° FOV, and can support up to a 20° FOV with relatively high performance. The previous microscope system could only support a diffraction-limited 5° FOV, so this would be a significant step forward,

and would also be able to have an even larger usable FOV than the ARMPM.

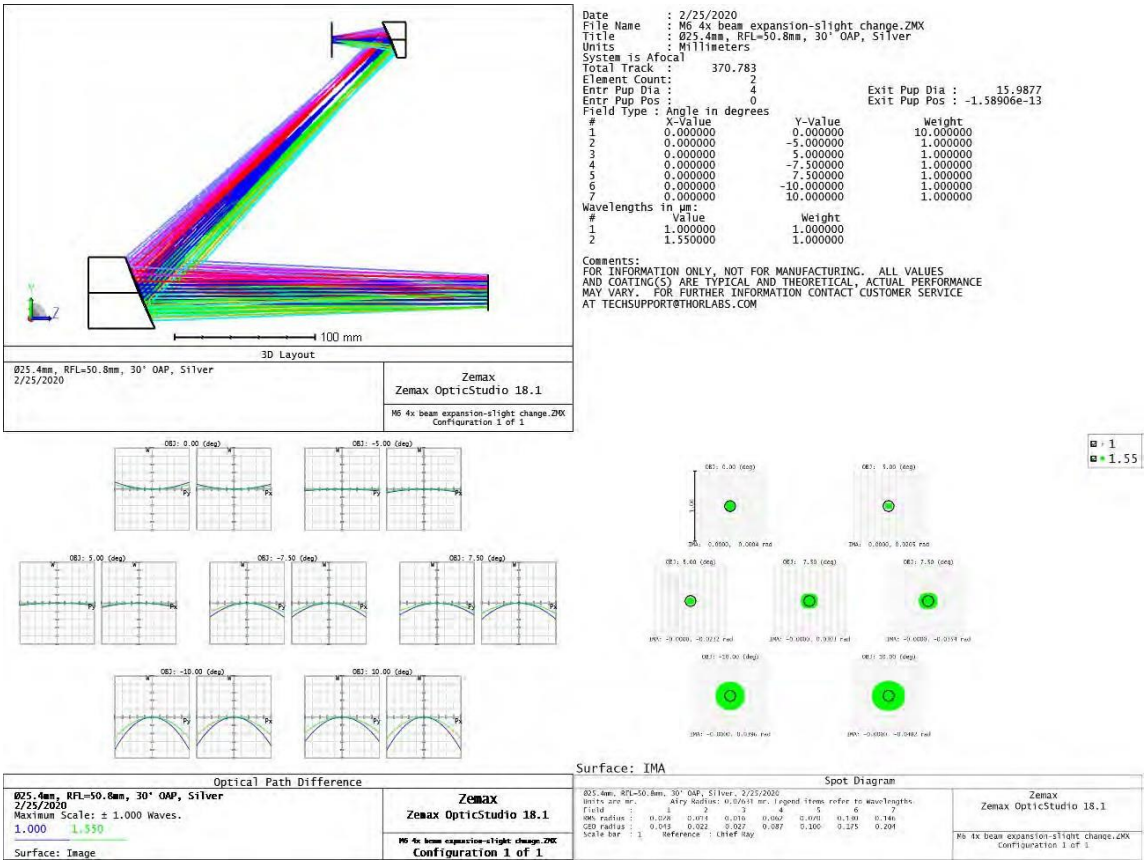

Figure 16: 4X beam expansion design with OAPs.

To further increase the model realism, a model of the reflective collimator from Thorlabs was used in OpticStudio to collimate the light to add the effect of its performance on the system. In addition, the beam scanning action of the galvometric mirrors was added via the multi-configuration editor tool of Zemax OpticStudio. This is an important step since this accurately models the beam footprint on the mirrors. Simply having the light scanned via a perfect pupil ignores the effect of the separation of the two scan mirrors on the final position of the

relayed pupil. Nine configurations were made, modelling the performance of on-axis light and the eight points forming a square in angle space of a 10 degree FOV. Several fold mirrors were added, including the one that sends the light into the microscope objective to accurately see how the beam might clip at different edges. This model is shown in Fig. 17. Gaussian beam apodization was applied to the beam leaving the fiber to further include these important effects.

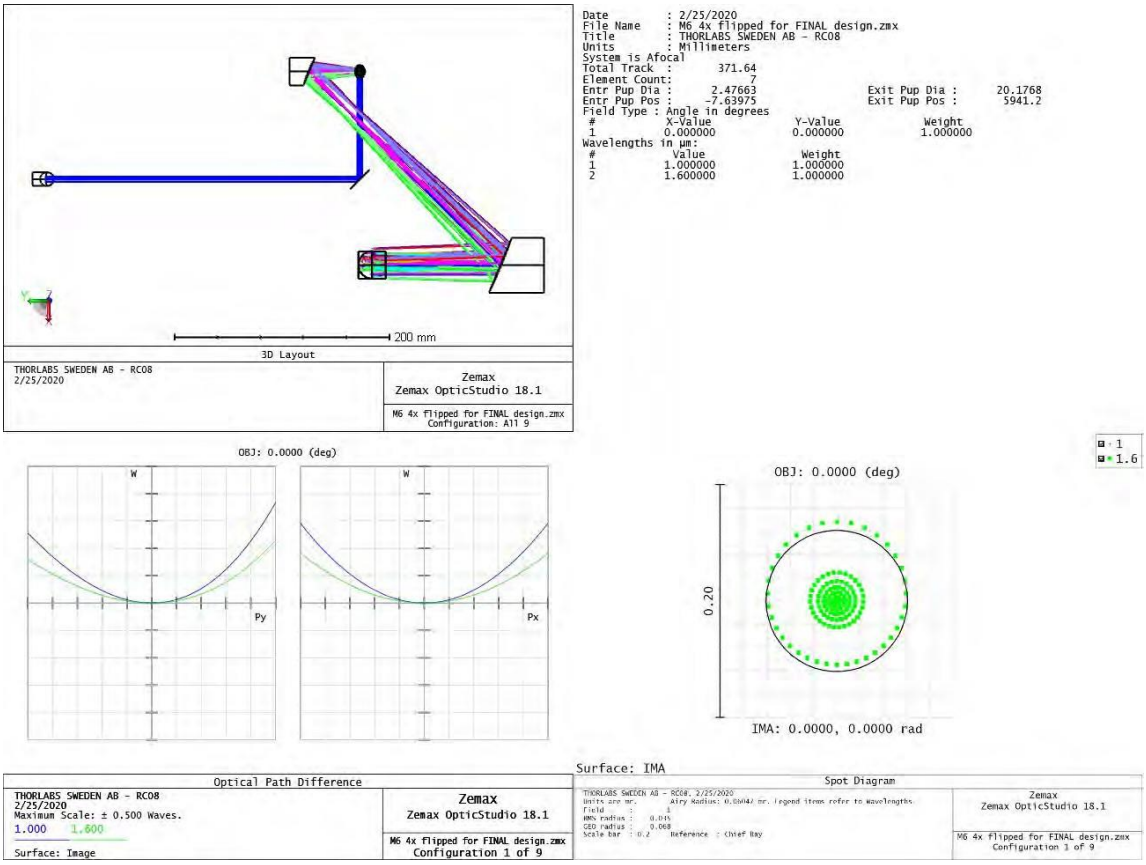

Figure 17: Advanced model using multi-configuration editor and the light beginning from the fiber.

Lastly, a tolerance analysis was performed in order to see how the system would behave under realistic assembly conditions. A summary of the tolerances used is shown in Table 2 below. The tolerances were set to initial values before an inverse sensitivity analysis was performed to see what values would still allow for a diffraction-limited system, or a wavefront error of less than a quarter wave.

Table 2: Tolerance values used in OpticStudio analysis

Type	Surface	Min shift	Max shift

Separation between scan mirrors and 2” OAP	Scan mirrors	-2 mm	2 mm
Separation between 2” OAP and 8” OAP	2” OAP	-2 mm	2 mm
X Decenter	2” OAP	-2 mm	2 mm
Y Decenter	2” OAP	-2 mm	2 mm
X Tilt	2” OAP	-1.68°	2°
Y Tilt	2” OAP	-1.11°	1.11°
X Decenter	8” OAP	-2 mm	2 mm
Y Decenter	8” OAP	-2 mm	2 mm
X Tilt	8” OAP	-1.01°	1°
Y Tilt	8” OAP	$-.86^{\circ}$	$.86^{\circ}$

This analysis indicated that the system was relatively tolerant to perturbations. With the exception of tilt on the two OAPs, especially tilt “out of plane” in the Y direction, the system can tolerance millimeters of positioning error. The output from the Monte Carlo run used to produce this chart, run with 10,000 iterations, is shown in Fig. 18 below. A typical metric for the “as-built” performance of a system post-tolerance analysis is the nominal performance plus two standard deviations. This gives a final wavefront error of .154, or almost an 1/8 of a wave at $1\mu m$. Even the mean plus 2σ is .253, or a quarter wave. This analysis gave high confidence that this system would be able to perform well in the real world. This allowed the system to proceed to the next phase of the design.

```
Number of traceable Monte Carlo files generated: 100000

Nominal         0.03491077
Best            0.03499559   Trial  18257
Worst           0.47115775   Trial  75193
Mean            0.13200294
Std Dev         0.06031938

98% >       0.27604638
90% >       0.21494557
80% >       0.18213650
50% >       0.12346376
20% >       0.07709209
10% >       0.06000563
 2% >       0.04323776
```

Figure 18: Output of Monte-Carlo simulation from inverse sensitivity analysis

Microscope System Design

In order to accommodate the multiple modalities, it was necessary that this microscope be more complex than previous systems. It would need to take the two inputs from the laser described in the previous chapter and combine them into one such that the two beams are co-linear into the system. It would need to have multiple detector systems for all three imaging modes: multiphoton, Raman, and brightfield. Ideally, it would also be a compact system in order to stay competitive in volume with the compact size of the ARMPM. However, ideally it should also been easy microscope to modify for future students to add even further capabilities. As such, this microscope is purposefully not as tightly packed as the previous ARMPM, while still being efficient in its use of space.

System Overview and Schematic Diagram

A schematic diagram of the complete optical system is shown in Fig.19 below.

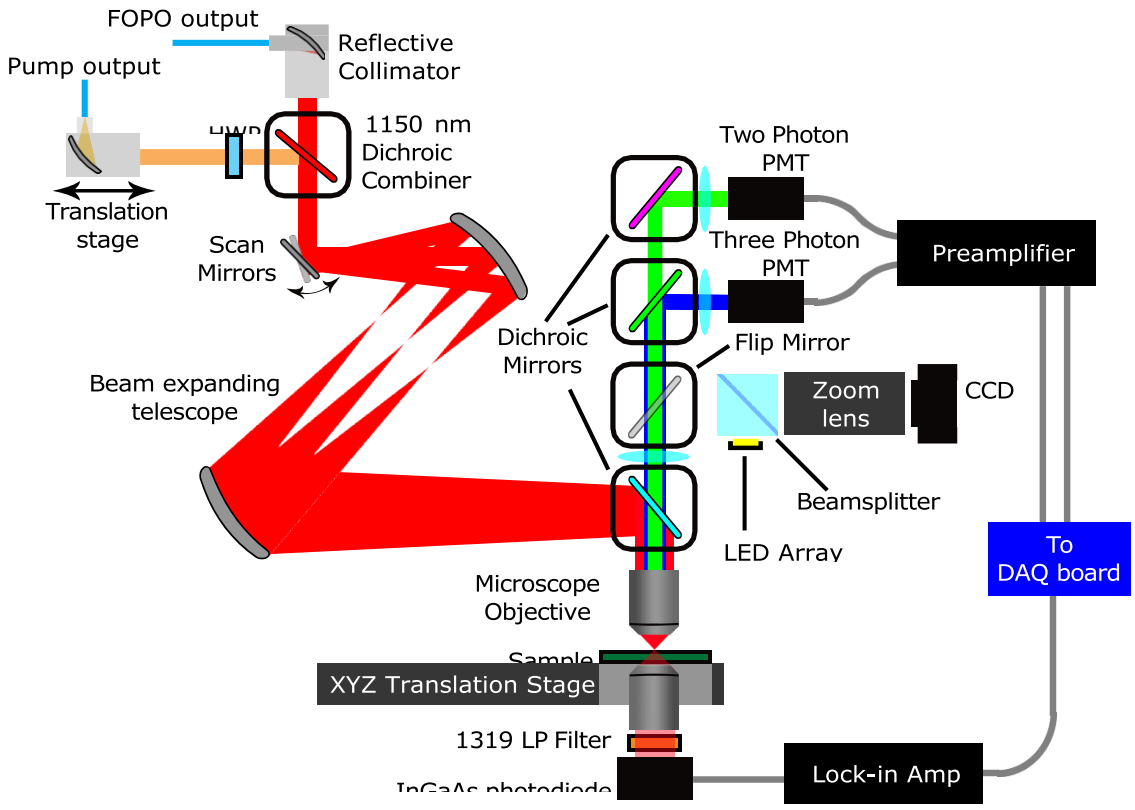

Figure 19: Schematic diagram of the M6 system. All components are labelled.

The system begins with the two fiber outputs from the laser described in the previous part collimated by Thorlabs reflective collimators (RC04APC-P01). It is worth noting that this system can take any ultrafast laser input, and does not depend solely on the new laser. A 1030 nm half-wave plate (Castech) is used to re- orient the polarization of the pump beam to that of the FOPO output. While both output fibers use PM fiber, this was still necessary to correct for the orientation of the collimator. An 1150 nm long-pass dichroic mirror (Semrock) is used to combine the beam. The pump output is placed on a translation stage in order to synchronize the pulse trains in time with each other. After the beams are combined, they are sent to the galvometric scan mirrors (Thorlabs GVS012). After this, the 2" OAP (Thorlabs MPD124-P01-45) and the 8" OAP (Thorlabs MPD284-P01-45) relay the pupil and expand the laser beam by a factor of 4, as described in the previous section. The light passes through an 830 nm dichroic mirror before being focused down onto the sample via a reflective microscope objective. At the sample, the multiphoton, Raman and other interactions would occur. While these effects are typically forward phase-matched, the signal is collected in epi-detection, and the Raman is collected underneath the objective via a second microscope objective (Mitutoyo 20x .4 NA NIR). After this objective, a 1319nm long-pass filter (Semrock) is used to allow only the output from the OPO to pass, since this will be carrying the Raman signal. The light is then picked up by an InGaAs photodiode, and sent to a Lock-in Amplifier (Zurich Instruments) that is synchronized to the signal from the AOM.

The multiphoton light is collected above and focused down through various filters and dichroics depending on the desired signal. Hamamatsu PMTs (10721-20 and 10721-110) are used to detect the light. While the first iteration of M6 has only two PMTs in use, there is sufficient space designed into the microscope box to allow for the use of 4 PMTs. The output from these PMTs is sent to a current preamplifier (Stanford Research 570) before being detected by the computer.

The brightfield signal is collected by a zoom lens (Tamron) and focused onto a CMOS array (Thorlabs DCC1645C-HQ). This zoom lens was needed to allow for shifting the focus of the incoming light, since it would already be slightly converging because of the lens right after the first dichroic mirror. A linear actuator will push a 45° prism mirror in and out of the beam to flip between nonlinear imaging and brightfield imaging modes.

Opto-mechanical Design

In order to lay out all the parts, a Solidworks model of the design was created using parts downloaded from the Thorlabs website, and designed parts when the original part file could not be found. A labelled view of the microscope is shown in Fig. 20. This model is shown with all the component parts including advanced fea- tures to show that they can indeed fit in the space allocated for them. For example, the ASI FW-1000 automated filter wheel, which works with the same controller box as the XYZ stage, fits well between the fiber input assemblies and the 2” OAP. In addition, the system is shown with four PMTs instead of two, clearly showing that they all fit. To give a sense of scale to this image, each hole on the breadboard is one inch apart. The upper breadboard is 12x18 inches (Thorlabs MB1218) and the lower breadboard is 18x24 inches (Thorlabs MB1824). The decision was made to mount the OAPs via specially designed mounts from Thorlabs, and to mount them directly to the breadboard. This was done in order to remove the variables of position and angle by placing them precisely via CNC machined holes in the breadboard.2

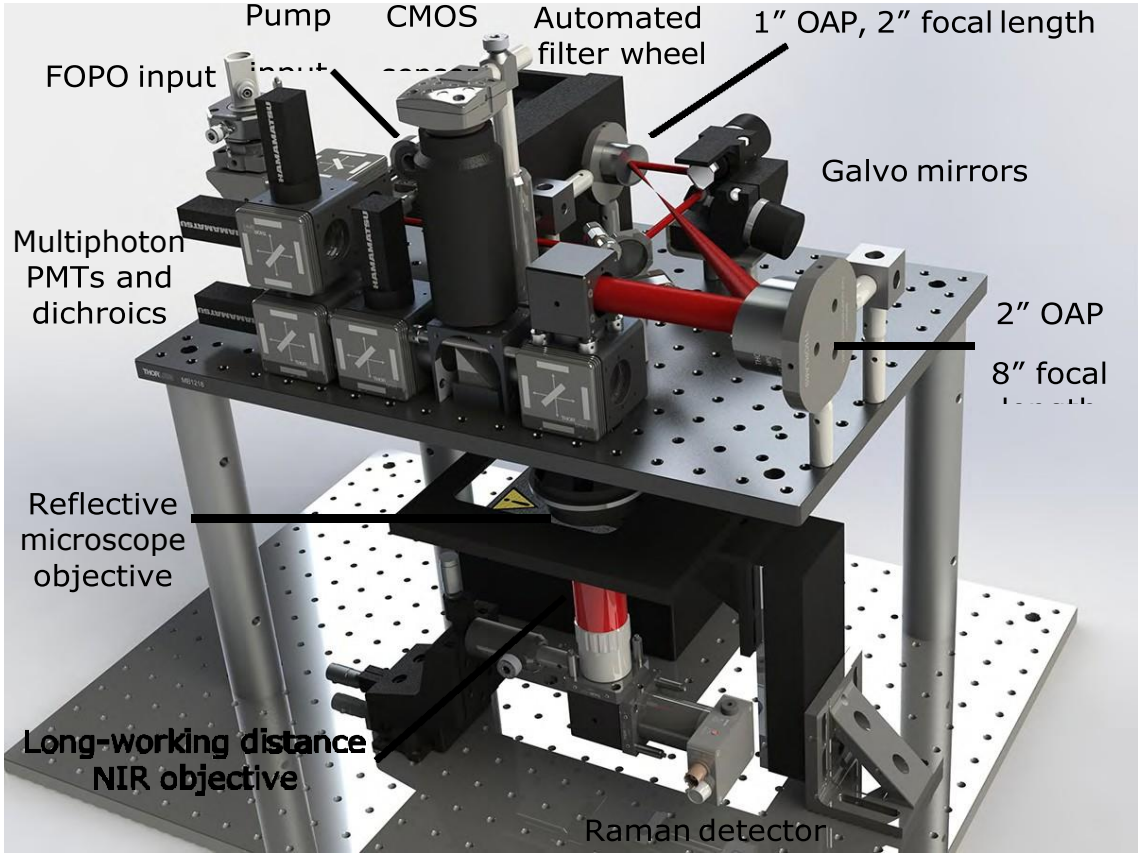

Figure 20: Rendered Solidworks model of the M6 system. Major components are labelled.

To more easily follow the role of each portion of the microscope, another version of the system was color-coded to highlight the four key segments of the system. The laser beam manipulation optics, including the beam expanding telescope and fiber delivery system, were colored red. The brightfield imaging system was colored yellow. The multiphoton detection components were colored green, and the Raman detection components were colored blue, seen in Fig. 21 below.

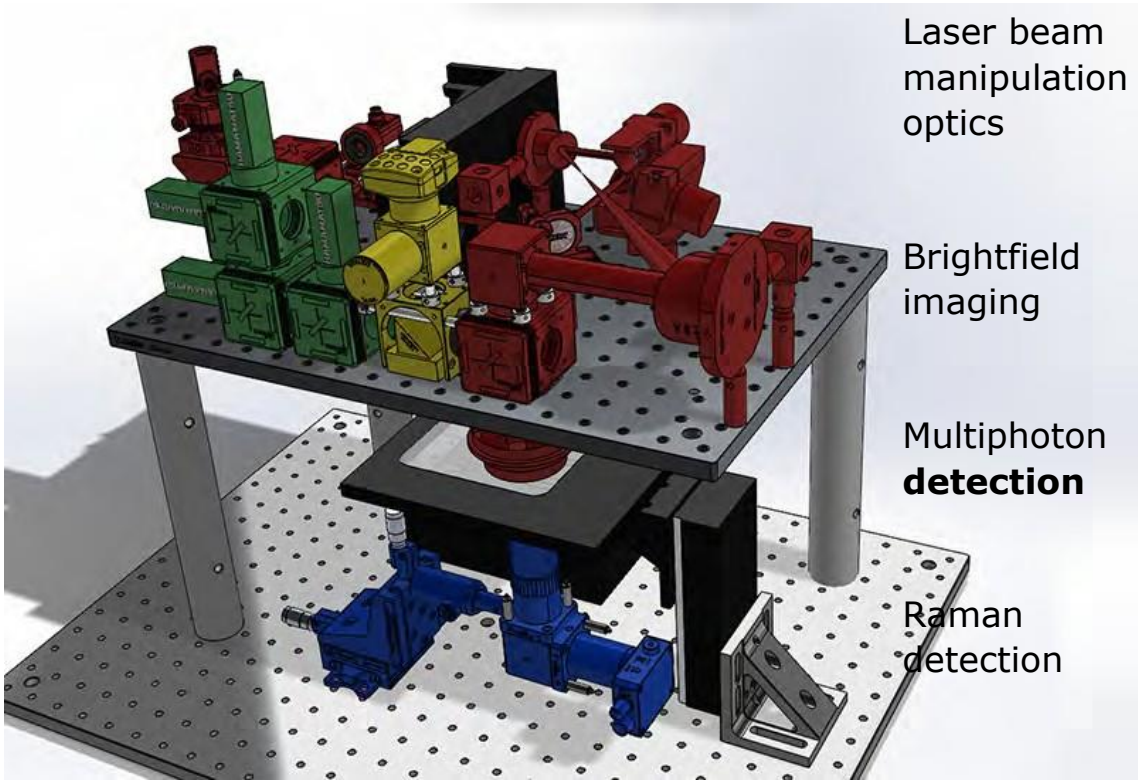

Figure 21: Color-coded Solidworks model, with color key.

Brightfield Imaging System Design

The design of the brightfield imaging system for this microscope was explored originally in OPTI585 with Prof. R. John Koshel. Several changes to the original design were necessary from the work done in that class. One aspect that was not explored in that class was the risk of ghost images on the detector through the beamsplitter that could drastically decrease the image quality. This was explored in early prototyping with a bright white light source seen in Fig. 4.8. Despite the AR coating on the beamsplitter, bright ghost reflections can be

seen from the sources. When the camera was placed here for testing, the light overwhelmed the sensor.

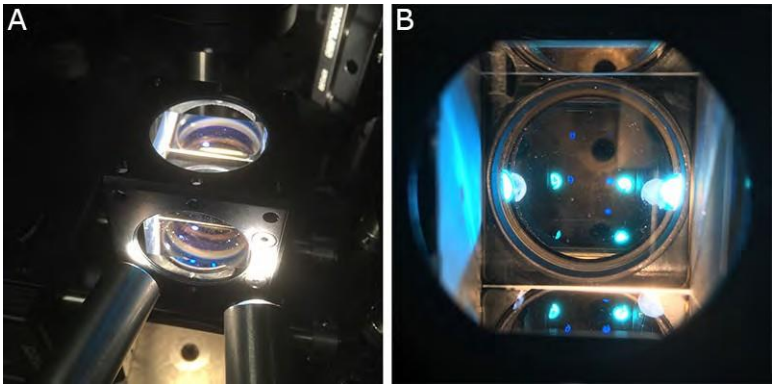

Figure 22: A: Two fiber coupled white light sources are incident on the side of the beamsplitter where the LED source would be injected. B: Top down view from the camera's perspective, showing the many ghost reflections despite the AR coating on the beamsplitter.

Based on this prototyping, the design choice was made to replace the inline lighting with lighting near the sample. Since this component of the microscope is mostly for convenience and not for high resolution imaging, a low-cost CMOS sensor (Thorlabs DCC1645C) and zoom lens (Tamron) were used. The zoom lens was chosen to account for the different microscope objectives, and the focus adjust knob would also relax the positioning tolerances on the vertical position of the detection assembly.

Raman Detection Design

For the Raman detection subsystem, a relatively simple optical design was needed. Like the PMTS, this is not an imaging detection system, the light just needs to make it to the detector. For this section, a few key filters needed to be selected. It was critical that only the light from the OPO made it to the detector, and not the much stronger pump signal in order to ensure the weak modulation from the SRS signal was captured. A collection of key filters for Raman detection are shown in Fig. 23 below.

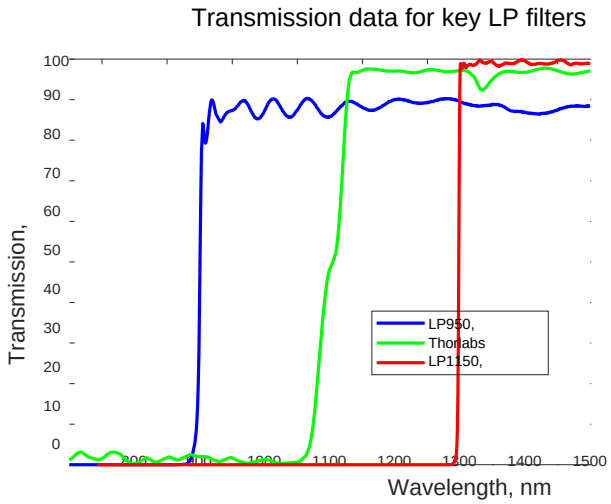

Figure 23: Key filters for the Raman detection with their transmission plotted as a function of wavelength.

LP950 is placed at the output of the OPO beam to block any of the signal light near 800 nm from entering the microscope system. LP1150 is the dichroic that combines the two beams. LP1319 is placed in front of the Raman detector after the microscope objective to block the pump light from reaching the detector.

Two of these filters are placed there, making the transmission of light near 1030 nm less than .00003%. The NIR Mititoyo 20x 0.4 NA objective was chosen as the collimating objective because of its long working distance and high transmission in the NIR range. A Newport XYZ translation stage is used to position the assembly at the correct position to be underneath the objective, and the right height to collimate the beam. The objective sends the collected light into the following optical system seen in Fig. 24 below. Two achromats (Thorlabs AC254-060-C) focus the light onto the detector.

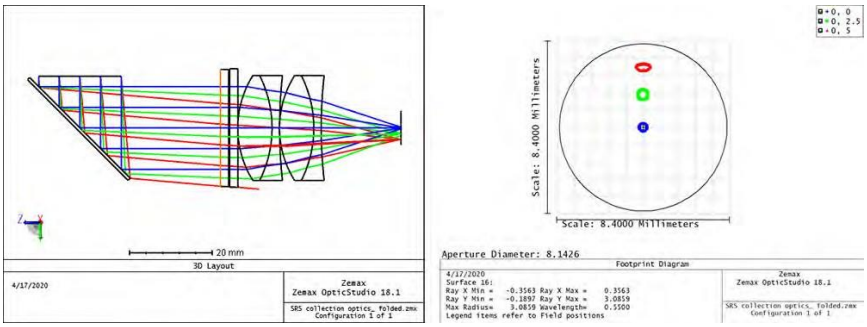

Figure 24: Left: Layout of SRS detection optics. A fold mirror sends the light through the two LP1319 filters before passing through two achromats and focusing onto the detector. Right: footprint diagram indicating where each FOV would come to focus off axis.

Generally, detectors with a fast temporal response or a short rise time have smaller active areas. Since the detector needs to resolve the repetition rate of the AOM, the detector used in this system needs to be relatively fast. In order to ensure a sufficiently fast detector would be able to detect light from the large FOV of M6, the footprint of focusing was important to consider, as shown on the right side of Fig. 24. The current detector in use is slower, but has a large active area and very low noise.

Assembly and Testing

Once the final optomechanical design was approved, the system was assembled. A large box was made in order to cover the microscope system, preventing room light from overwhelming the PMTs. The design went through several modifications in order to optimize the placement of various components. Currently, only two PMTS are in use, and the filter wheel is not in place while nonlinear imaging testing is performed. The assembled system is seen using the new laser in Fig. 25 below. The Raman detection system can be seen underneath the XY stage.

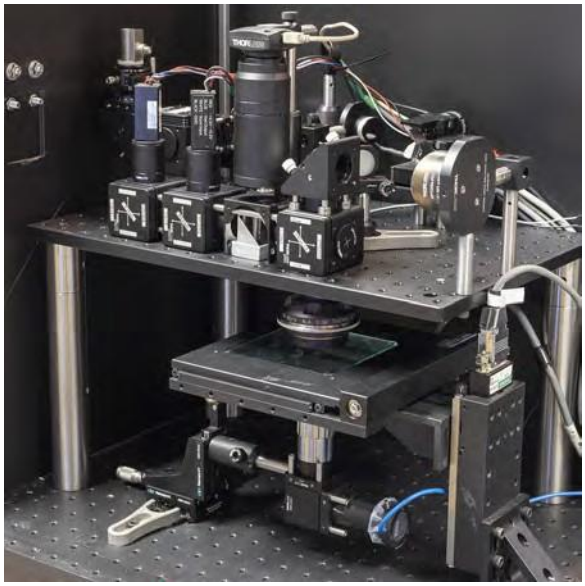

Figure 25: The assembled M6 system.

A labelled top-down view is also included in Fig. 26, since the front line of components obscures much of the rest of the system. This view also shows the galvanometric mirror power supplies at the bottom of Fig. 26, which are attached to the underside of the top breadboard in order to save space.

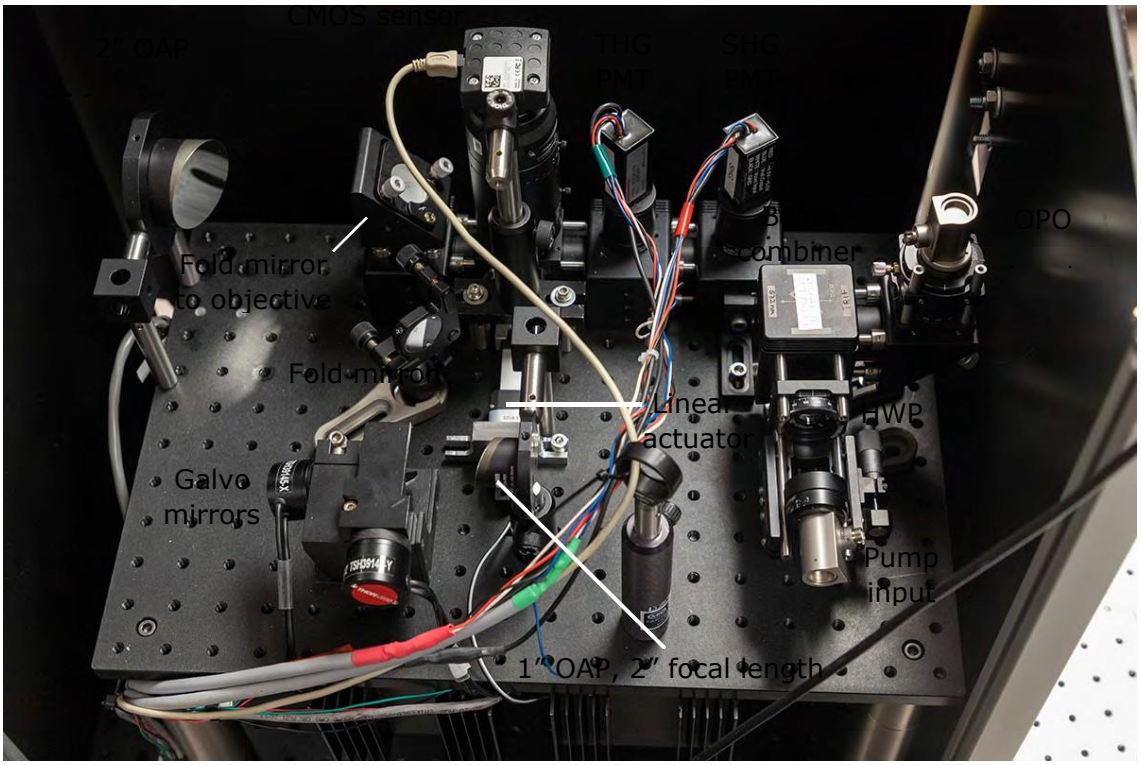

Figure 26: Labelled top-down view of M6.

Translation Stage Re-design

In the initial rounds of testing, it was discovered that the translation stage could have a small impact on the focus position between the two beams. Fig. 27 demonstrates this. When the translation stage (Thorlabs CT1, 0.5 inch travel) was moved between the two edges of its travel, the focus position would shift by around $6\mu m$. As a result of this, this translation stage would not be able to be used to synchronize the pulses in time. This is a manifestation of Gaussian beam optics, as the laser beams are not truly collimated. To address this, a fiber coupled optical delay line was added to the laser before the AOM in order to synchronize the pulses in time.

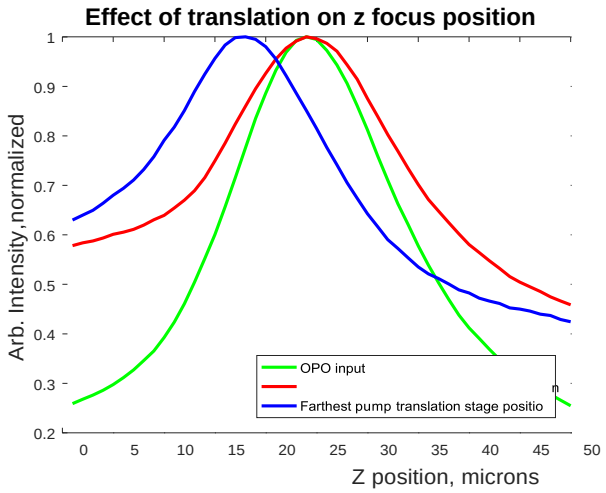

Figure 27: The position of the translation stage could change the focus positions

Using the free space Agilent 86100A Wide-band oscilloscope, the time overlap between the OPO pulse and the pump pulse could be measured. The tap from the oscillator was used as the trigger for the oscilloscope using an ET-5000F InGaAs PIN detector from Electro-Optics Technology, and a multimode optical fiber was used to collect the two laser beams after being combined in free space. This fiber delivered the two beams to the 30GHz optical channel for detection, giving a 30 picosecond resolution. Since the laser pulses are both on the order of 5 ps, some fine tuning would still be needed on the delay stage to maximize the signal. The recorded traces from the oscilloscope can be seen in Fig. 28 below.

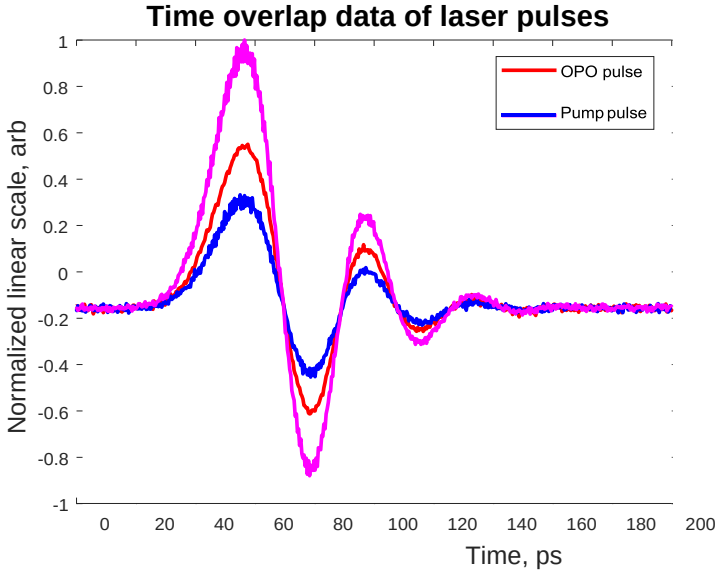

Figure 28: Data from the oscilloscope indicating that the pulses are overlapped.

Performance Characterization

The microscope was characterized using our nonlinear-knife edge technique using the edge of a piece of Gallium Arsenide (GaAs) developed in our group. Briefly, to extract the resolution values, we model the signal intensity across the edge as a summation of a step function representing the wafer edge and a delta function representing the SHG signal from the edge. From this measurement, we see near-diffraction limited performance is achievable, with the average resolution between the two channels at 1.18x the diffraction limit (Fig. 29). The degradation in the performance from the diffraction limit is a combination of aberrations in the M6 design and the commercial reflective microscope objective.

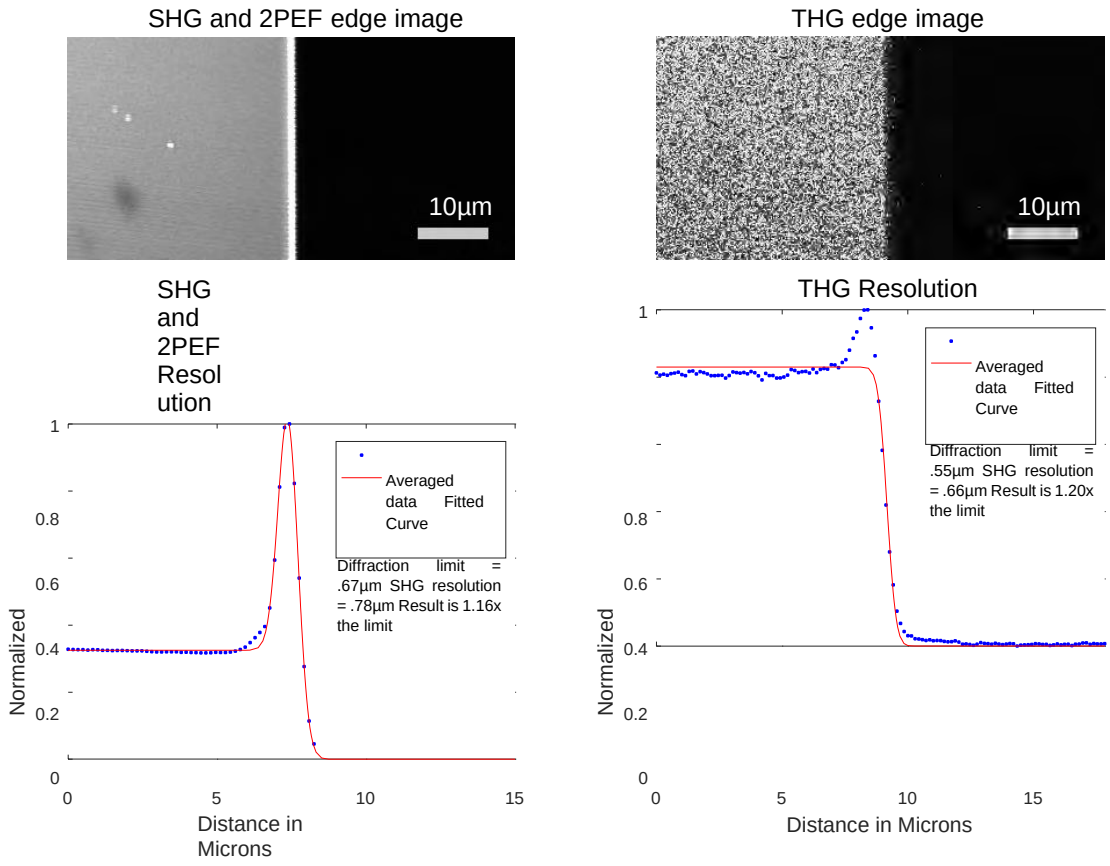

Figure 29: Nonlinear knife-edge resolution test resolution using the 1040 nm laser and the 15x 0.58 NA Reflachromat from SpectraTech, showing performance of ≈ 1.18x the diffraction limit

Imaging Results

The microscope has been used for several imaging projects so far. A collection of images using the full field of view on the microscope is shown in Fig. 30 below. These images were taken with a 20x. 0.75NA Nikon S Fluor objective with the 1560nm laser. The field of view with this 20x objective was measured using a slide micrometer to be $580\mu m$ across.

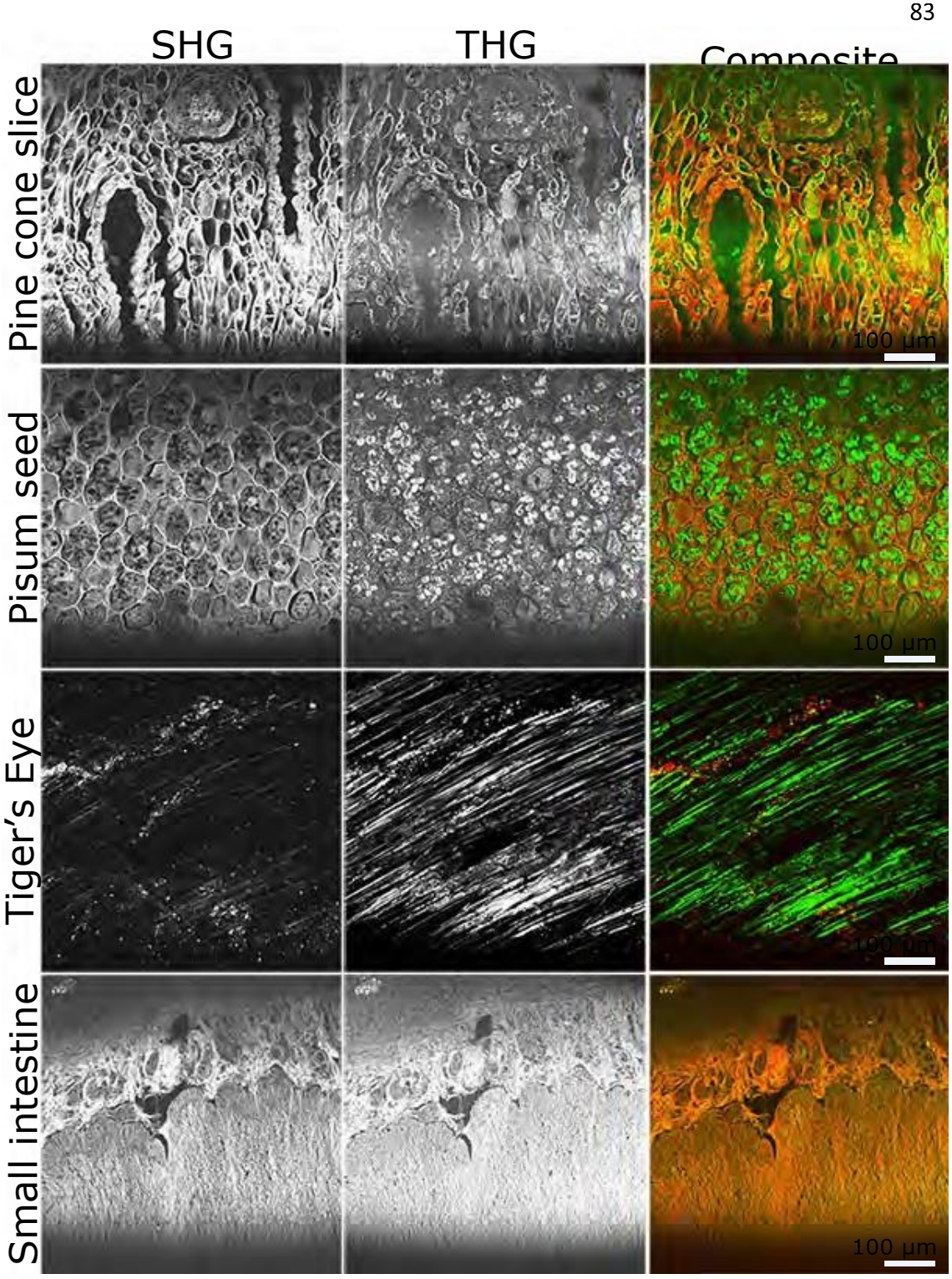

Figure 30: Collection of images from M6, broken into the 2 photon and 3 photon channels and combined in false color. The sample labels are on the side. Some vignetting can be seen on the bottom of the images.

Like the other microscopes, M6 can capture interesting features in 3D as well. A z-stack of a prepared mosquito slide is shown in Fig. 31 below. The stack is not very deep since the mosquito was placed between two glass slides, making it only slightly less than 200μm thick. This is by no means the limit to the depth imaging of the microscope.

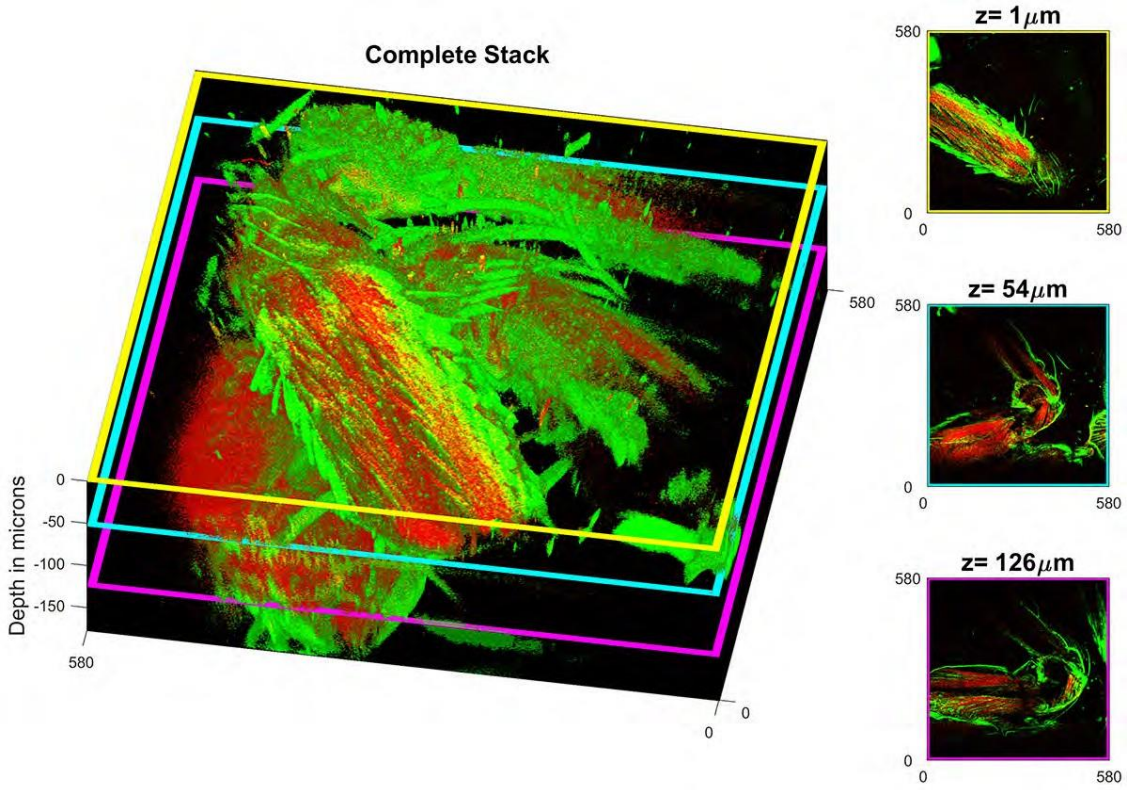

Figure 31: 3D rendering of a z-stack of a prepared mosquito slide, as well as highlighted depths on the side. This portion of the mosquito includes several joints, where the SHG/2PEF highlights the muscles of the insect, and the THG highlights the exoskeleton.

These images do show some slight vignetting due to using a spherical mirror as the fold mirror instead of an elliptical mirror, which would increase the vertical FOV. This mirror was used out of availability and replacing it with an elliptical mirror will remove this vignetting issue. One concern discovered in the testing process is the presence of smile distor- tion in the microscope system. An image simulation in OpticStudio confirmed the images first seen on the system. Fig. 32 shows both the image simulation and an uncorrected image of a computer chip. Fortunately, as distortion is an error in ray height mapping and not a defocusing term, this can be corrected in software.

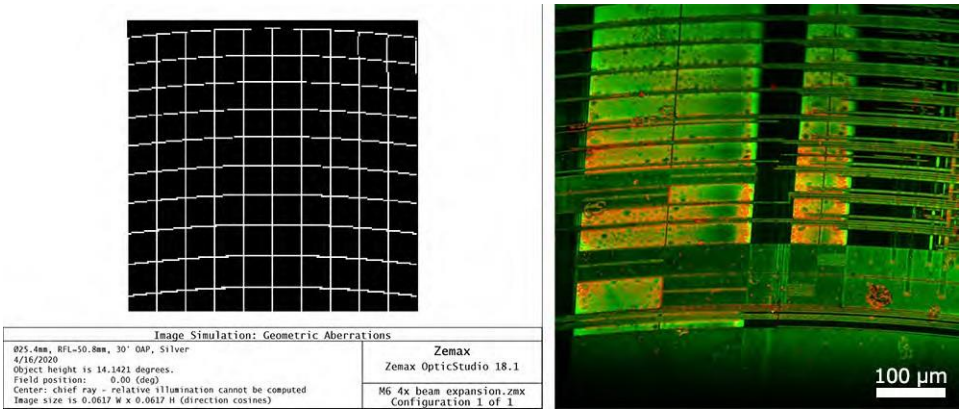

Figure 32: Left: OpticStudio image simulation of a grid of lines, clearly indicating smile distortion. Right: An uncorrected image of a computer chip taken at the full FOV of M6. The straight lines on the chip help to clearly illustrate the distortion.

Unexpected Signal from GaAs Sample

Interestingly, the all-reflective imaging system has created signal unexpectedly from the Gallium Arsenide (GaAs) slices used in our group for microscope alignment and testing. An example image is shown in Fig. 33 below.

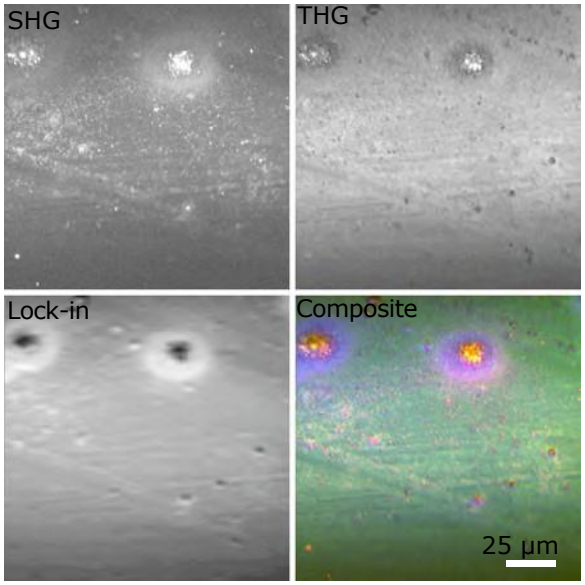

Figure 33: Signal seen from the GaAs sample with SHG, THG, and potentially FWM in the Lock-in channel. The three are combined in false color on the right, with the SHG in red, the THG in green, and the Lock-in signal in blue.

The GaAs slice was being used for alignment on the multiphoton arm when a strong signal was noticed in the Raman channel. However, the separation between the pump and OPO beams was set to be for the biological resonance near $2950 cm^{-1}$, far from any of the GaAs resonances in the fingerprint region. The signal on the lock in depends on both lasers being synchronized in time, space, and polarization, but does not seem to be strongly wavelength selective. Because of the polarization sensitivity of the signal, it is possible that this signal was a result of four-wave mixing (FWM), another $\chi^{(3)}$ effect with similar phase matching conditions to SRS, but without as much wavelength sensitivity. This signal was very strong, showing over 40dB above the noise floor on a spectrum analyzer.

Another interesting feature of this signal is that the signal does not maximize until well below the top surface of the GaAs, seen in Fig. 34 below.

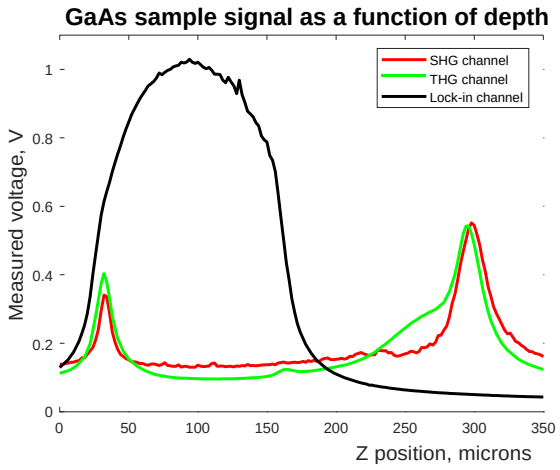

Figure 34: Intensity averaged across the images over the course of a z-stack for all three signals. The peaks for SHG and THG correspond to the top and bottom surfaces of the GaAs slice.

The peaks for SHG and THG indicate where the top and bottom surfaces of the GaAs slice are found, yet the signal from the lock-in does not maximize until another $70\mu m$ or so, and maintains a large signal over a much larger depth than either of the other signals. This signal has been seen in both GaAs and Silicon samples. The GaAs signal is polarization dependent, while the Si signal is polarization dependent to a much lesser degree. Further experiments are needed to flesh out and understand the source of this signal.

Conclusion

This part has thoroughly described the design and characterization of a new mirror-based laser scanning microscope, M6. The optical and mechanical designs were discussed, and the schematic and key parts of the microscope system were described. Resolution and performance characterization were discussed, and images from all three imaging modes were presented.

This microscope, especially when combined with the laser described in the previous chapter, will be a highly versatile and capable tool for future projects. Fig. 35 highlights the complete journey of this concept, from optical design file to completed physical system. Further detail on the assembly instructions and mechanical drawings can be found in the M6 Technical Data Package (Please contact the PI for this).

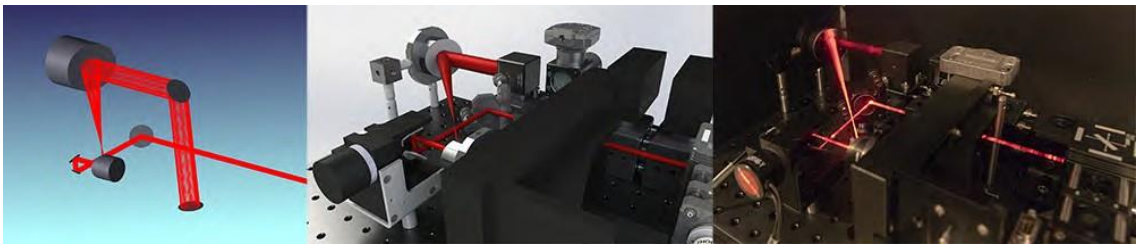

Figure 36: M6, from Zemax design to Solidworks model to completed system. The image of the completed system with the red laser was captured using a long exposure image and a piece of paper to trace out the beam.